

Vital Sign and Sleep Monitoring Using Millimeter Wave

ZHICHENG YANG, University of California, Davis

PARTH H. PATHAK, George Mason University

YUNZE ZENG, XIXI LIRAN, and PRASANT MOHAPATRA, University of California, Davis

Continuous monitoring of human's breathing and heart rates is useful in maintaining better health and early detection of many health issues. Designing a technique that can enable contactless and ubiquitous vital sign monitoring is a challenging research problem. This article presents mmVital, a system that uses 60GHz millimeter wave (mmWave) signals for vital sign monitoring. We show that the mmWave signals can be directed to human's body and the Received Signal Strength (RSS) of the reflections can be analyzed for accurate estimation of breathing and heart rates. We show how the directional beams of mmWave can be used to monitor multiple humans in an indoor space concurrently. mmVital also provides sleep monitoring with sleeping posture identification and detection of central apnea and hypopnea events. It relies on a novel human finding procedure where a human can be located within a room by reflection loss-based object/human classification. We evaluate mmVital using a 60GHz testbed in home and office environment and show that it provides the mean estimation error of 0.43 breaths per minute (Bpm; breathing rate) and 2.15 beats per minute (bpm; heart rate). Also, it can locate the human subject with 98.4% accuracy within 100ms of dwell time on reflection. We also demonstrate that mmVital is effective in monitoring multiple people in parallel and even behind a wall.

CCS Concepts: • **Human-centered computing** → **Ubiquitous and mobile computing systems and tools**; • **Applied computing** → *Health care information systems*; • **Hardware** → *Signal processing systems*

Additional Key Words and Phrases: Millimeter wave, 60 GHz, vital signs, human finding, signal reflection and blockage, healthcare, smart home

ACM Reference Format:

Zhicheng Yang, Parth H. Pathak, Yunze Zeng, Xixi Liran, and Prasant Mohapatra. 2017. Vital sign and sleep monitoring using millimeter wave. *ACM Trans. Sen. Netw.* 13, 2, Article 14 (April 2017), 32 pages.

DOI: <http://dx.doi.org/10.1145/3051124>

1. INTRODUCTION

Monitoring vital signs such as breathing rate and heart rate can provide crucial insights in a human's well-being and can detect a wide range of medical problems. Continuous and ubiquitous monitoring of a person's vital signs is a challenging problem and the current solutions require the person to wear dedicated devices. Wearable devices such as wrist-worn heart rate monitors, chest straps for breathing rate detection are required to be connected to the human's body at all times (even during sleep), making them a less convenient alternative. This has motivated the design of contactless solutions

Authors' addresses: Z. Yang, Y. Zeng, X. Liran, and P. Mohapatra, Department of Computer Science, University of California, Davis, Davis, CA 95616; emails: {zcyang, zeng, xliran, pmohapatra}@ucdavis.edu; P. H. Pathak, Department of Computer Science, George Mason University, Fairfax, VA 22030; email: phpathak@gmu.edu.

Permission to make digital or hard copies of part or all of this work for personal or classroom use is granted without fee provided that copies are not made or distributed for profit or commercial advantage and that copies show this notice on the first page or initial screen of a display along with the full citation. Copyrights for components of this work owned by others than ACM must be honored. Abstracting with credit is permitted. To copy otherwise, to republish, to post on servers, to redistribute to lists, or to use any component of this work in other works requires prior specific permission and/or a fee. Permissions may be requested from Publications Dept., ACM, Inc., 2 Penn Plaza, Suite 701, New York, NY 10121-0701 USA, fax +1 (212) 869-0481, or permissions@acm.org.

© 2017 ACM 1550-4859/2017/04-ART14 \$15.00

DOI: <http://dx.doi.org/10.1145/3051124>

for vital sign monitoring where a person's smartphone or other nearby communication infrastructure (e.g., WiFi) can be leveraged for the purpose.

In the RF-based vital sign monitoring solutions proposed in Liu et al. [2015], Patwari et al. [2014], Abdelnasser et al. [2015], and Ravichandran et al. [2015], a WiFi signal reflected from the human body is used to estimate the breathing and heart rates. Although these papers have solved important challenges in designing contactless vital sign monitoring, they have many practical limitations. Due to the omni-directional propagation commonly used in 2.4/5GHz WiFi, a signal can be reflected from multiple humans in an indoor space. This makes it difficult to distill the vital signs of multiple humans from the reflected signal. Due to this reason, the majority of the WiFi-based vital sign monitoring research assumes there is only a single human subject in the range of WiFi endpoints, or if there are multiple humans in the range, their vital signs are sufficiently different from each other. However, in most practical scenarios, there is more than one human in indoor spaces like homes, offices, and hospitals, and the vital signs of individuals can vary substantially in a short time. The WiFi signal can also reflect from many indoor objects, and complex signal processing is necessary to extract the human reflected signal in multi-path rich indoor environments. This makes it difficult to determine the tiny motion of heartbeats from the reflected signal and, hence, the approaches in Patwari et al. [2014], Abdelnasser et al. [2015], and Ravichandran et al. [2015] are primarily limited to measuring only the breathing rate.

This article investigates the use of 60GHz millimeter-wave (mmWave) signal for ubiquitous and non-invasive vital sign monitoring. The 60GHz mmWave frequency band provides over 7GHz (57–64GHz) of unlicensed spectrum. With the development of IEEE 802.11ad [IEEE 2012], the mmWave band is shown to enable high-speed (up to 7Gbps) indoor wireless local/personal area networks. Its suitability for applications, such as point-to-point video streaming, has resulted in rapid commercialization with the development of WiFi+60 GHz wireless access points [Intel 2014], smartphone chipsets, and the like. With this momentum, the 60GHz mmWave is likely to be an omnipresent technology of indoor WLANs/WPANs in homes and offices in the coming years. We demonstrate that the 60GHz mmWave signal can provide highly accurate and reliable vital sign monitoring. Due to the high attenuation loss of 60GHz signal, directional beamforming is employed using a phased array or horn antenna to concentrate the signal in one direction. We show that mmWave signals reflected off a human body can accurately represent minute chest motion necessary to estimate his/her breathing and heart rate. Due to the directional nature, the signal is not affected by any other motion outside the transmitter (Tx) and receiver (Rx) beams. Even more importantly, the directional beams reduce the signal footprint of monitoring each human, which in turn allows higher spatial reuse where multiple human subjects can be monitored in parallel within a room.

In this article, we present mmVital, a comprehensive vital sign and sleep monitoring system using mmWave. mmVital can measure a human's breathing rate and heart rate in different positions (standing, sitting, sleeping, etc.) without requiring any proactive actions from the human. It is robust to different distances and incident angles of the impinging signal, as humans can change their locations anywhere in the room. In addition to vital signs, mmVital can also monitor a person's quality of sleep with identifying sleeping postures, because frequent changes in posture is found to be correlated with the quality of sleep [Oksenberg and Silverberg 1998]. Another important factor to impact the sleep quality is the breathing disorder. For this purpose, mmVital can accurately detect apnea events for patients suffering from sleep disorders such as central apnea and hypopnea.

mmVital solves multiple challenges toward building a practical monitoring system. With mmWave, it is necessary to perform Tx and Rx beamforming toward the human in order to reflect the signal off his/her body. To address this challenge, mmVital utilizes

a *human finding* process where the indoor surrounding is profiled and monitored in terms of mmWave reflections. The human finding procedure results in accurate beam-forming angles to point and reflect the signal from human(s). We identify the separation conditions that dictate how multiple humans can be monitored using mmWave and how mmVital can provide very high concurrency of monitoring compared to the omni-directional WiFi-based solutions. This feature can facilitate parallel monitoring of multiple patients on nearby beds in a hospital room or different family members in a home. This can be easily implemented on the future commercial 60GHz devices, which are supposed to be multiple nodes in a typical living environment due to high-power loss at 60GHz. These devices can form reflective paths bounced from/to a human body to enable our proposed work. The contributions of this article can be summarized as follows:

- (1) We empirically demonstrate the feasibility of the monitoring of breathing and heart rates using 60GHz mmWave signals. We develop a state-of-the-art testbed and design mmVital, a vital sign monitoring system that utilizes Received Signal Strength (RSS) of the mmWave signal reflected from a human to provide accurate vital sign monitoring while being robust to different incident angles and distances.
- (2) We develop a contactless sleep monitoring system that does not require the user to wear any devices on his/her body during sleep. mmVital can monitor a person's sleep by identifying sleeping postures and detecting the posture changes. It also observes human's breathing patterns during sleep for detecting sleep apnea events (specifically, central apnea and hypopnea). We note that research presented in this article is an extension of our previously published work [Yang et al. 2016a]. Compared to the work of Yang et al. [2016a], the novel contribution of this work is the development and evaluation of sleep monitoring techniques, including posture classification and apnea detection.
- (3) A novel *human finding* technique is developed that can be used by mmVital to locate a user based on the reflection loss of a human body. We develop a reflection loss-based classification that can accurately and efficiently distinguish reflection from a human body or other objects (e.g., walls and chairs).
- (4) We systematically study and empirically derive the (angular and distance) separation necessary between humans for concurrently monitoring their vital signs. Additionally, we establish the relationships between the necessary separation and the antenna beamwidth, and outline possible cases such as blockage, multiple reflections, and the like.
- (5) We do an extensive evaluation of mmVital using our 60GHz testbed with seven participants in office and home environments. The mean estimation error across all participants is observed to be 0.43 breaths per minute (Bpm) and 2.15 beats per minute (bpm). The human finding procedure achieves object-human classification accuracy of 98.4% with 100ms of dwell time on reflection changes. mmVital is also accurate in behind-the-wall breathing rate estimation with the mean estimation error of 0.58Bpm.

The rest of the article is organized as follows. Section 2 discusses the related work. Section 3 provides the overview of mmVital, and Section 4 discusses the breathing rate and heart rate estimation modules. Section 5 represents the posture event detection and classification, and apnea detection modules. Section 6 details the human finding procedure, and Section 7 discusses the monitoring of multiple people. Section 8 provides the numerical results, and we conclude in Section 9.

2. RELATED WORK

RF signal-based contact-free solutions for vital sign and sleep monitoring have received increasing attention in recent years. Our work is related to the prior works in the

following three areas, 2.4/5GHz band and mmWave band for sensing as well as the sleep apnea monitoring systems.

2.4/5GHz-based vital sign monitoring: The authors in Abdelnasser et al. [2015] proposed to use WiFi RSS for respiratory monitoring. However, it requires the person to hold a device or stand in the line-of-sight path between Tx and Rx nodes for accurate monitoring. Liu et al. [2015] leveraged fine-grained Channel State Information (CSI) of WiFi to track vital signs. The primary focus of the work is to measure the vital signs when a person is sleeping and the approach is applicable to monitoring a single person in a controlled environment. Also, the proposed solution can only monitor multiple humans when their vital signs are sufficiently distinct. However, in practical scenarios, individual's vital signs can vary substantially in a short time period. A similar work [Ravichandran et al. 2015] studied a natural setting in the home with both Line-of-Sight (LOS) and Non-LOS (NLOS) cases to estimate a single person's respiration rate using customized WiFi hardware. The work is limited to measuring breathing rate (not heart rate) and can only monitor multiple humans' breathing rates when they are sufficiently different. The authors in Huang et al. [2016] proposed a self-calibrating vital sign monitoring system based on the Doppler radar; however, the required demodulation procedure only focused on the case of single subject monitoring.

Authors in Prakash et al. [2016] developed a Global System for Mobile communications (GSM)-based Internet of Things (IoT) network to monitor vital signs, in which computational and network processors are interfaced with sensing components and transmit signals through GSM and Simple Mail Transfer Protocol (SMTP) servers. Different from mmVital, the vital sign sensors in Prakash et al. [2016] are required to be attached to users. A wireless sensor system using 802.15.4 devices was proposed to monitor vital signs in Patwari et al. [2014], which requires the deployment of many sensor nodes/links for the accurate monitoring of a single human. Adib et al. [2015] proposed to use Frequency-Modulated Continuous-Wave (FMCW) radar for breathing and heart rates estimation. The proposed work can monitor multiple human subjects in parallel. However, it utilizes a customized dedicated hardware with a large bandwidth of 1.8GHz (between 5–7GHz). In contrast, mmVital can reuse the IEEE 802.11ad commercial communication/networking hardware for the purpose of vital sign monitoring. Although we use customized mmWave platform (due to the unavailability of off-the-shelf hardware), our techniques simply rely on RSS and can be easily implemented on low-cost future commercial 60GHz Wireless Local Area Network (WLAN) devices.

mmWave sensing and networking: While some research has found that the exposure under mmWave might moderately increase human skin's temperature [Gandhi and Riazi 1986; Wu et al. 2015], mmWave is otherwise shown to have no significant detrimental effects on the human body [Price 2012], given that the transmission power and antenna gain are carefully chosen as per the regulations [Rappaport et al. 2014]. Previous works have also studied vital signs detection using the mmWave signal in different frequencies, such as 228GHz [Petkie et al. 2009], 94GHz [Mikhelson et al. 2012; Bakhtiari et al. 2012] and 60GHz [Kao and Lin 2013; Chuang et al. 2012]. The primary focus of these papers has been to demonstrate the feasibility of vital sign monitoring with mmWave. They assume simple controlled settings with one human subject at a close distance from the transmitter and receiver. In addition, Bakhtiari et al. [2012] and Chuang et al. [2012] focused on mmWave sensor and hardware/chip design for vital sign detection. In our work, our focus is on solving practical challenges such as finding the human's location in a room and realizing the true potential of directional beams by sensing multiple humans concurrently. mmVital is designed to be operational in realistic indoor environments like offices, homes, and so on as shown in our evaluation.

In the literature, 60GHz millimeter wave sensing has been studied extensively for other applications like target tracking and automotive radar. In a recent work, Wei

and Zhang [2015] proposed the high-precision tracking of objects (writing with pen) using mmWave beam scanning. The reflection characteristics of different objects for mmWave signals have been studied in Langen et al. [1994]. Authors in Sur et al. [2015] provided a link level measurement of blockage and reflection in an indoor environment, and our reflection measurements closely match their results due to the similarity of 60GHz transmitter and receiver system. 60GHz communication has been studied for outdoor picocells [Zhu et al. 2014] with its reflection and absorption characteristics, for wireless links in data center networks [Zhou et al. 2012] and for WLANs [Nitsche et al. 2015] with beamforming assisted via out-of-band 2.4/5GHz WiFi. The reflection, blockage, and beam-steering characteristics studied in these works are in agreement with our work.

Sleep monitoring systems: Polysomnography is a commonly used clinical test to diagnose the sleep apnea disorder [Spriggs 2014], whereas it requires the patient to attach multiple sensors during sleep in the hospital. To overcome this inconvenience issue, Kayyali et al. [2008] showed a home-based polysomnography system for monitoring sleep disorders, rather than the conventional polysomnography equipment where subjects are required to sleep in a hospital laboratory. Masa et al. [2011] proposed a home respiratory polygraphy, a cost-effective home-based sleep monitoring system, for the diagnosis of sleep apnea-hypopnea syndrome. Furthermore, some portable and/or mobile device-based sleep monitoring systems have also been developed in recent times. Mamelak and Hobson [1989] mounted transducers on a headband to monitor sleep states by predicting non-rapid-eye-movement and rapid-eye-movement. Rofouei et al. [2011] developed a wearable neck-cuff system for real-time monitoring of sleep disorders, which consists mainly of a neck cuff and a cellphone/computer with Bluetooth wireless communication. Fullpower [2014] designed a mobile application for sleep apnea, snore, heart rate, and weight loss monitoring. Nguyen et al. [2016] presented a wearable sleep staging monitoring system that uses an in-ear recorder to evaluate bio-electrical brain wave signals. However, all of the approaches above still require either a variety of specialized sensors or mobile devices attached to the subject.

The authors in Mack et al. [2009] developed a ballistocardiography-based monitoring system to monitor breathing, heartbeat, and musculoskeletal movements. Shin et al. [2010] used balancing tubes to evaluate the performance of an air mattress sensor system on monitoring heart rate, breathing rate, snoring events, sleep apnea, and body movement of the subject. Norman et al. [2014] validated a mattress-based monitoring system that detects sleep disordered breathing behaviors without sensors attached to the subject. Although subjects are not required to wear sensors in these methods, the mattresses are customized to embed various pressure sensors. The authors of Nandakumar et al. [2015] recently proposed to use sound wave with FMCW to measure breathing and detect apnea events, in which the smartphone running the application needs to be placed close to the subject. Our non-intrusive approach based on mmWave wireless signals does not require any other additional sensors attached to subjects, or any modification of the sleeping furniture. It can be easily coupled with future 60GHz WLAN devices.

3. SYSTEM DESIGN

We now describe our 60GHz communication platform, design goals, and challenges and provide an overview of mmVital.

3.1. mmWave Communication Platform

mmVital is implemented using a 60GHz transmitter and receiver which use a mmWave development platform provided by Vubiq [Pasternack 2015]. The mmWave platform provides a 60GHz RF front end and a waveguide module as shown in Figure 1. On

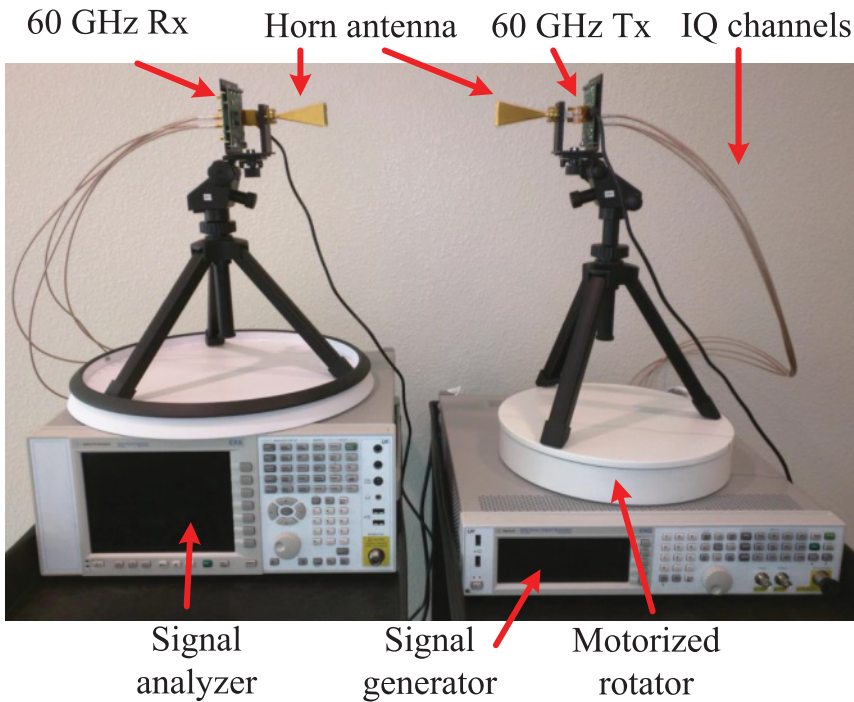


Fig. 1. mmVital 60GHz transmitter and receiver system.

the transmitter side, we use a signal generator (Keysight EXG N5172B) that produces a 10MHz baseband sine wave signal that is input to the Vubiq transmitter module. On the receiver side, the 60GHz receiver module is connected to a spectrum analyzer (Keysight EXA N9010A) that allows us to analyze the received baseband signal. We calculate the RSS using the power spectral density distribution provided by the spectrum analyzer. The RSS values are available at an average of 62 samples per second in experiment setup, which is sufficient for monitoring breathing and heart rates. Due to the unavailability of any reconfigurable phased array, we use a horn antenna with 3dB beamwidth of 12° (estimated First Null Beamwidth (FNBW) of 24°) and 24dBi gain on the transmitter and receiver. A mechanical rotator is used to form the beams in different directions and scan the surroundings for reflections.

3.2. Design Goals and Challenges

To compensate for the high attenuation loss, 60GHz radios use directional antenna (e.g., horn antenna or phased array). The central objective of mmVital is to exploit the directional nature of mmWave communication to accurately measure a human's breathing and heart rates. The mmWave Tx directs its signal to the human body and the reflected signal is received by the Rx. In terms of design, mmVital should be able to exploit the directional nature of mmWave and measure the vital signs of *multiple humans* concurrently. mmVital should be *non-invasive*, which means that it should not require the human to perform any specific actions to monitor the vital signs. mmVital should also be *ubiquitous* where the monitoring can be performed anywhere within the reach of Tx and Rx. Additionally, the monitoring should be accurate even when the human is sleeping, standing, or sitting, and should be robust to different postures (front, back, right, and left).

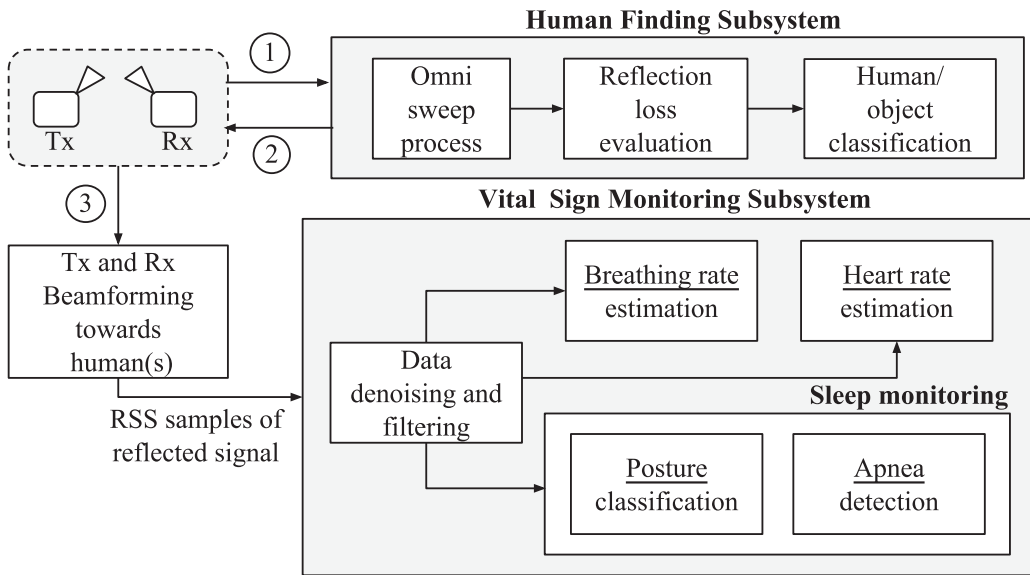


Fig. 2. Overview of mmVital.

Although the directional nature of 60GHz communication reduces the inaccuracies introduced by other motions and indoor multi-paths, it also raises multiple challenges:

- (1) Because a human can be at different places compared to the Tx and Rx, it is necessary that the reflection-based monitoring is robust to different incident angles of signal onto the human body and different postures (front, back, left, right) of the body. We study the impact of incident angle and body postures on vital sign monitoring, and also develop a technique to identify sleep postures and detect sleep apnea.
- (2) Before starting the vital signs monitoring, it is first required to *find* the human in the vicinity of Tx and Rx. Since various indoor objects (e.g., wall, metal cabinet) reflect the mmWave signal, mmVital needs to distinguish the reflections from objects and humans. Although this can be accomplished by inspecting each reflection for heartbeats, the time overhead of such inspection with many possible reflections indoors can be very high. We develop an algorithm for *human finding*, where the Tx and Rx engage in an iterative scanning to profile the indoor environment in terms of its current reflections, and inspect them to identify the reflection from a human body.
- (3) With narrow beamwidths, it is possible to use multiple non-overlapping beams to monitor the vital signs of multiple humans in parallel. The relative position of multiple humans results in many complex reflection scenarios such as the blockage of one human by the other or multiple reflections. We systematically classify various scenarios and study the angular and distance separation necessary for concurrent sensing.

3.3. System Overview

Various components of mmVital are shown in a block diagram in Figure 2. At a high level, mmVital contains two subsystems: (i) human finding subsystem and (ii) vital sign monitoring subsystem. The goal of the former subsystem is to find the human in a room (or an indoor space) so that Tx can direct its signal toward the human and

Rx can receive the reflection. For accomplishing this efficiently, mmVital utilizes an omni-sweep procedure that profiles the indoor environment in terms of its reflections and tracks any changes to it. When new reflections are detected, the reflection loss is evaluated to classify if they are from movable objects (e.g., chairs, laptops) or a human. mmVital leverages the diversity in material permittivity to accurately identify human reflections. Once the Tx and Rx beamforming angles toward the human are determined, the second subsystem performs the vital sign monitoring.

The signal reflected by the human body is analyzed through RSS samples to estimate the vital signs. The RSS samples first undergo a data denoising procedure where a sliding window-based moving average filter is applied to remove the high-frequency noise. Apart from that, we also apply a bandpass frequency filter with cutoff of 0.1–20Hz in order to remove the impact of a slow moving DC component as well as moderate to high-frequency human movements [Munguia Tapia 2008] (e.g., shaking of body parts).

The filtered RSS samples are then used by four separate modules. The breathing rate and heart rate modules further apply their custom filters and peak detection algorithms (discussed in the next section) for estimation. The filtered samples are also utilized by the posture module to identify a user's current sleeping posture. The apnea detection module monitors a human's breathing pattern to detect any central apnea or hypopnea events. We note that posture classification and apnea detection do not require estimating vital signs, and hence, can operate separately and in parallel. We first provide the details of a vital signs subsystem in the next section and defer to the discussion on a human finding subsystem to Section 6.

4. MEASURING VITAL SIGNS

4.1. Breathing and Heart Rates

In order to estimate the breathing rate, we transform the filtered RSS data to the frequency domain. We observe that the RSS signal is very sensitive to the periodic movement of human breathing, which results in a peak (dominant frequency) in the frequency domain. The frequency of the peak represents the breathing rate at a coarse-grain. However, simply selecting the highest peak is not always accurate due to variations introduced by noise and motion. To achieve a better accuracy, we select the highest-magnitude peak as well as the frequency of the two adjacent bins and create a custom narrow band-pass filter. We apply the filter on the RSS data and perform an Inverse FFT (IFFT) to yield the filtered time-series data. We then use a simple peak detection algorithm for precisely counting the breathing rate in Bpm.

The normal heart rate of an adult is known to be in the range of 60–100bpm [Ganong and Barrett 2005]. However, during high-intensity activities like exercising, the heart rate can exceed 170bpm [Ganong and Barrett 2005]. For such activities and to detect any other abnormal conditions, we select the heart rate range to be 50–220bpm. Similar to the breathing rate estimation, we apply an Fast Fourier Transform (FFT) on the RSS time-series data and determine the dominant frequency. In this case, we select the highest-magnitude peak along with four adjacent bins of frequency to create the custom band-pass filter because the heart beat motion is smaller than the breathing motion and can exhibit larger variations. We apply the filter, perform IFFT, and use the peak detection for estimating heart rate.

Figure 3 shows an example of raw RSS samples along with filtered breathing and heart beat samples. We offset the RSS values by the transmission power to present the RSS and RSS loss on the same scale. After applying the customized filters, we apply a peak detection algorithm for accurate counting. We note the mmVital estimates the vital signs in real time using a sliding window of 30 seconds offset by approximately 100ms (every six RSS samples in our testbed).

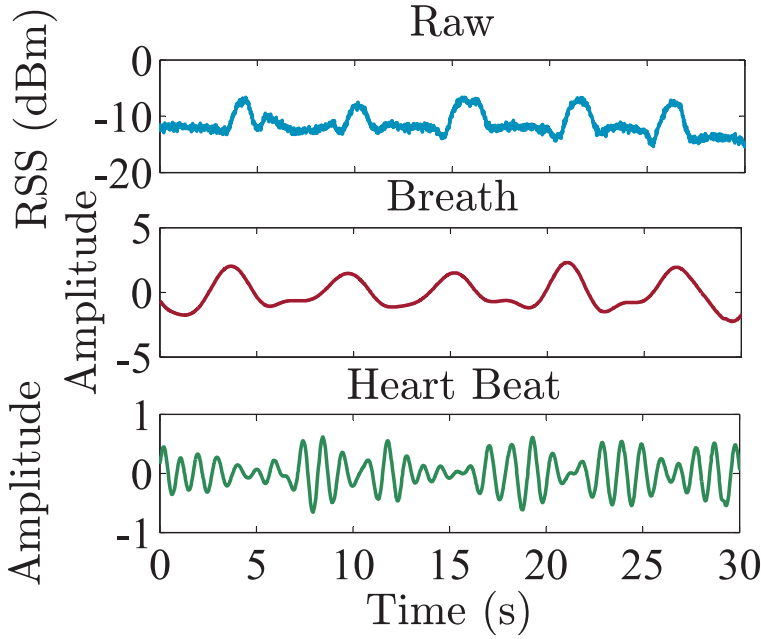


Fig. 3. Raw RSS of the reflected signal and extracted breathing and heart beats.

4.2. Impact of Incident Angle

Because a human can be anywhere within the Tx and Rx vicinity while being monitored for his/her vital signs, the transmitted signal can impinge on the human body at any angle (referred to as incident angle). We now investigate the impact of incident angle on the reflected signal and the robustness of breathing rate and heart rate estimation. The amount of energy reflected from an object can be quantified using a *power reflection coefficient* which can be derived from a reflection coefficient. The reflection coefficient is the ratio of the complex amplitude of the reflected electromagnetic wave to that of the incident wave. The coefficient depends on factors such as the permittivity (a complex value) of the object material and the signal incident angle. The reflection coefficient (r) can be calculated [Ahmadi-Shokouh et al. 2009] as

$$r = \frac{1 - e^{-j2\omega}}{1 - r_i e^{-j2\omega}} r_i, \quad \text{for } i \in \{\perp, \parallel\}, \quad (1)$$

where $\omega = \frac{2\pi l}{\lambda} \sqrt{\epsilon_2/\epsilon_1 - \sin^2 \gamma}$, l denotes the thickness of the reflecting source; λ denotes the signal wavelength; γ is the incident angle; and ϵ_1 and ϵ_2 are the permittivities of the first medium and the second medium, respectively. In a simplified single layer model, the first medium can be assumed as air, which has the permittivity of one. r_{\perp} and r_{\parallel} are the Fresnel's reflection coefficients when the electric field is perpendicular and parallel to the incidence plane, respectively. The coefficients can be calculated as

$$r_{\perp} = \frac{\cos \gamma - \sqrt{\epsilon_2/\epsilon_1 - \sin^2 \gamma}}{\cos \gamma + \sqrt{\epsilon_2/\epsilon_1 - \sin^2 \gamma}}, \quad (2)$$

$$r_{\parallel} = \frac{\epsilon_2 \cos \gamma - \sqrt{\epsilon_2 \epsilon_1 - \epsilon_1^2 \sin^2 \gamma}}{\epsilon_2 \cos \gamma + \sqrt{\epsilon_2 \epsilon_1 - \epsilon_1^2 \sin^2 \gamma}}. \quad (3)$$

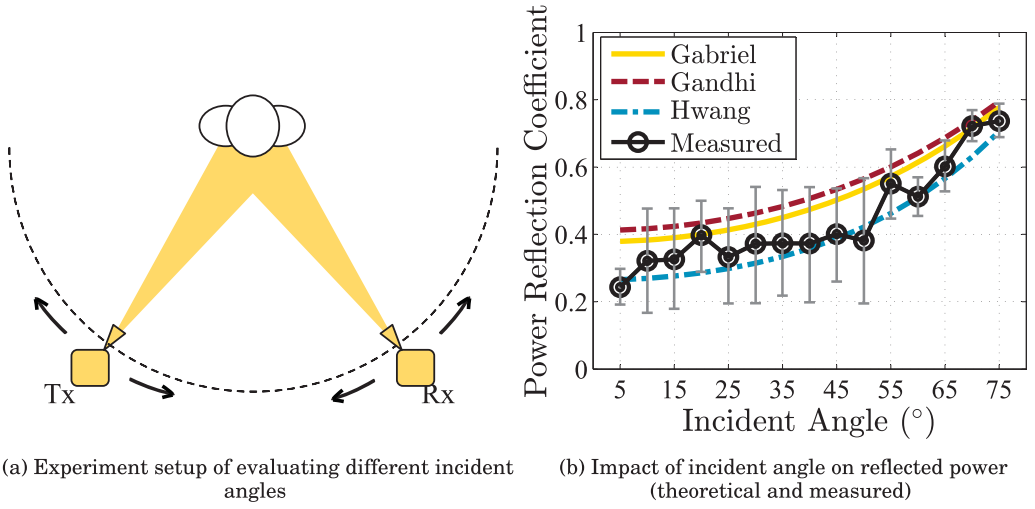


Fig. 4. The impact of incident angle: more transmitted signal power is reflected back to the receiver as the signal incident angle increases.

The reflection coefficient (r) can be used to estimate the power loss due to reflection (or power reflection coefficient) as $L_R = \frac{P_O}{P_I} = |r|^2$ where P_O and P_I are the values of reflected (after reflection) and incident (before reflection) power, respectively.

We empirically evaluate the impact of incident angle on the reflection power loss as shown in Figure 4(a). In the experiments, the Tx and Rx move symmetrically on a circle with a 3 meter radius. The human sits at the center of the circle, and both Tx and Rx point their horn antennas to the human. Since the P_I is unknown, we first use an aluminum plate at each incident angle in the place of the human and measure the received power. As an aluminum plate is regarded as a perfect reflector (reflection loss nearly 0dB), and we use its received power as a reference for human measurements. Figure 4(b) shows the reflection loss (L_R) for incident angles from 5° to 75° . It also compares the theoretical value of reflection loss calculated using Equations (1) and (2) (perpendicular). For the calculations, three different values of human body/skin permittivity are considered based on previous work from Gabriel et al. [1996], Gandhi and Riazzi [1986], and Hwang et al. [2003]. These values are $7.89 - j10.90$, $8.89 - j13.15$, and $8.05 - j4.13$ at 60GHz, respectively [Zhadobov et al. 2011]. We observe that our measurements are in agreement with the permittivity models of Gabriel et al. [1996] and Hwang et al. [2003]. Higher variations observed in the measurements are due to the human's breathing motion. Examples of the reflected RSS (raw and filtered) at different incident angles are shown in Figure 5. It can be seen that as the incident angle increases, the RSS samples become less and less noisy mostly due to the decrease in the reflection loss. The main observation in Figure 5 is that the reflected RSS is representative of the breathing motion at all incident angles. Hence, mmVital is robust to the human changing location relative to Tx and Rx. Also, if mmVital is used to monitor humans when they do not change their locations (e.g., sleeping in a bedroom or hospital bed), it is advisable to deploy the Tx and the Rx at larger incident angles to increase the estimation accuracy. We will evaluate the vital sign estimation accuracy for multiple human subjects with different incident angles in Section 8.

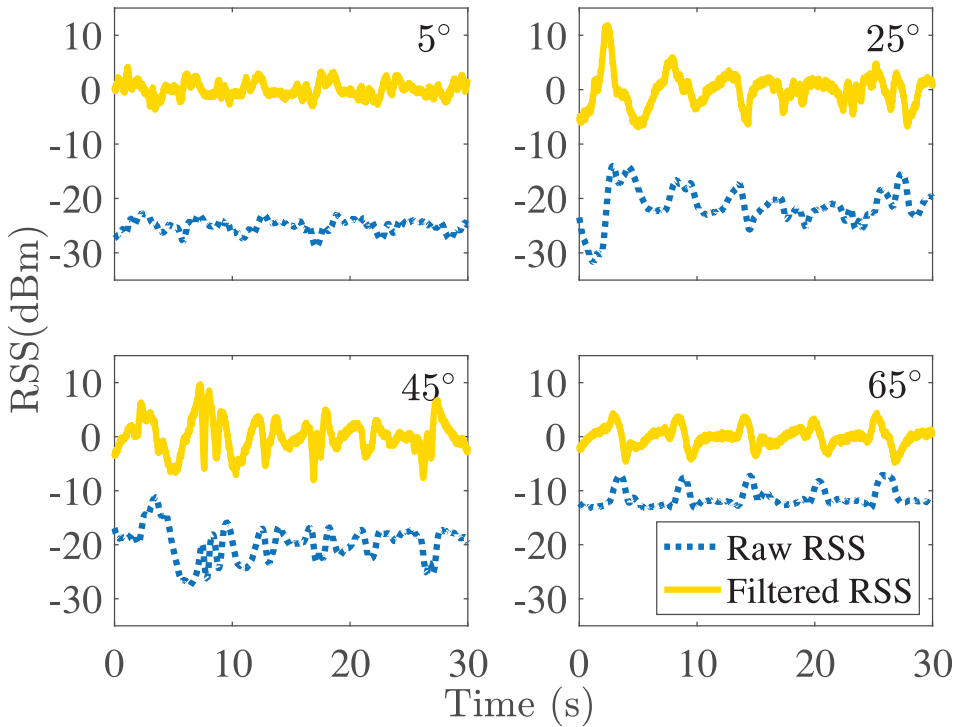


Fig. 5. Raw and filtered RSS for 5° , 25° , 45° , and 65° incident angles. The RSS samples are comparatively less noisy at higher incident angles due to reduced reflection loss.

5. SLEEP MONITORING

mmVital performs sleep monitoring through identifying a user's current posture and the detection of apnea events.

5.1. Posture Detection and Classification

Detecting the human's current sleep posture and posture change events is useful in determining the quality of sleep as well as sleep related disorders [Oksenberg and Silverberg 1998]. Sleep posture affects the breathing pattern and oxygen inhalation, and can aggravate existing sleep disorders such as apnea [Oksenberg and Silverberg 1998]. For example, a sleeping-on-stomach posture may cause some breathing obstruction that impacts the subject's breathing pattern and oxygen inhalation. In this work, we are primarily interested in detecting a human's sleeping posture and apnea events by observing the RSS of the reflected signal in mmVital.

mmVital utilizes the observed variance in the denoised RSS samples to detect posture change events. As shown in Figure 6, a typical posture change event causes considerable variation in the RSS for a certain amount of time. We leverage this observation to design a threshold-based technique that detects if the RSS variance is higher than a certain value for a given amount of time to determine a posture change event.

For the posture classification, we are interested in four sleep postures: sleeping on back (Front), sleeping on stomach (Back), facing left (Left), or facing right (Right). mmVital leverages the fact that when a wireless signal strikes the human body, the reflection is affected by the body posture. Figure 7 shows the frequency domain of the filtered RSS samples for a subject in four different postures. It is observed that

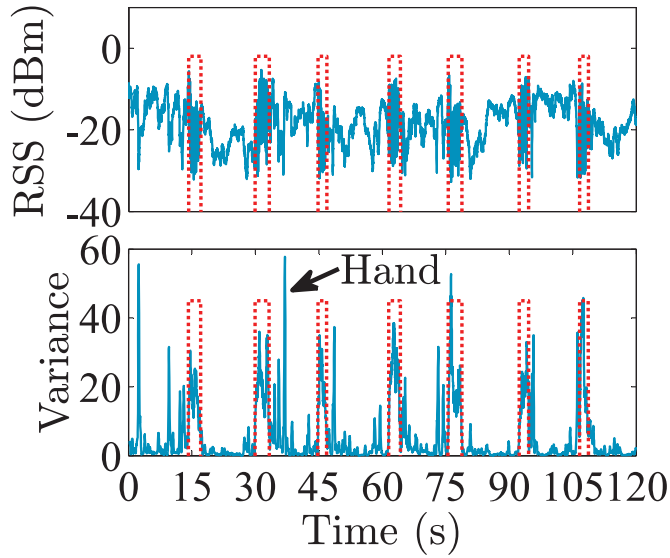


Fig. 6. An example of posture change event: posture change can be detected by monitoring the RSS variance for a pre-defined amount of time.

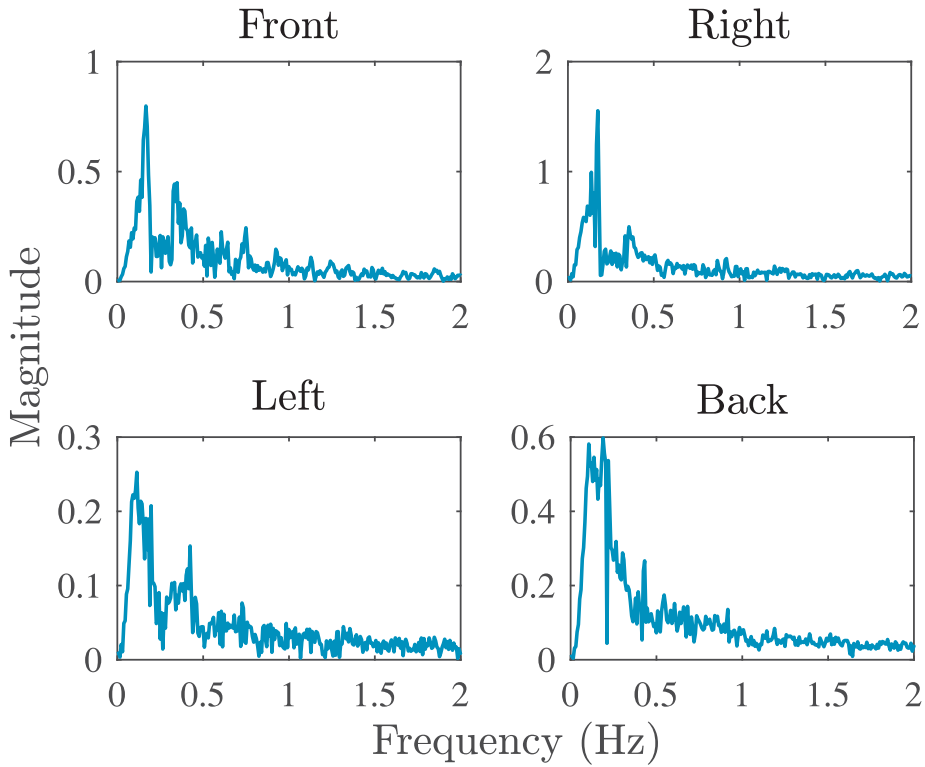


Fig. 7. Frequency domain analysis of RSS can be used to classify different postures.

Table I. Time Window Features (Time and Frequency Domains) Used for Posture Classification

Time domain	Mean Maximum Variance Range First, second, and third quartiles
Frequency domain	Energy (Equation (4)) Entropy (Equation (5)) Dominant frequency ratio Mean Variance

a signal reflected off the human's chest in facing right posture has a much higher magnitude than facing left. However, the difference in breathing motions in front and back postures cannot be observed through visual inspection. To classify among the four postures, we use a set of statistical features calculated over a moving time window of RSS samples. Table I lists the time and frequency domain features that we use in posture classification.

The dominant frequency ratio [Munguia Tapia 2008] is calculated as the ratio of the highest magnitude FFT coefficient to the sum of the magnitude of all FFT coefficients. The energy [Munguia Tapia 2008] is calculated as

$$Energy = \sum_{i=1}^{\text{window_length}/2} m^2, \quad (4)$$

where m is the magnitude of FFT coefficients. The entropy [Munguia Tapia 2008] is calculated as

$$Entropy = - \sum_{i=1}^{\text{window_length}} n_i \log_2(n_i), \quad (5)$$

where n_i is the normalized value of FFT coefficients.

Figure 8 shows the effectiveness of the selected features in posture classification. We observe that energy provides important indication about the posture. The energy reflects the position of human's heart compared to the Tx and Rx. When the human is facing right, his/her heart is closer to the signal's point of impact on the human body. The received signal is thus more sensitive to the chest movement caused by breathing and heart beats. Table II shows the standard deviation of four postures, in which the facing right posture has the largest value. In the frequency domain, facing right results in the highest observed energy in the reflected RSS. This is followed by front and back postures where reflection from the front exhibits more energy than from the back. When the human is facing left, least energy is observed due to his/her heart being farthest from the reflection point among all four postures. We build a decision tree-based machine learning classifier with the features described above, and mmVital uses the classifier to identify the user's current posture.

5.2. Apnea Detection

Apnea disorder is widely characterized as disruption in normal breathing pattern especially during sleep. It was shown in Nandakumar et al. [2015] that it affects over 18 million American adults with a variety of resulting disorders. There are two major types of breathing pattern changes that are associated with different types of apnea.

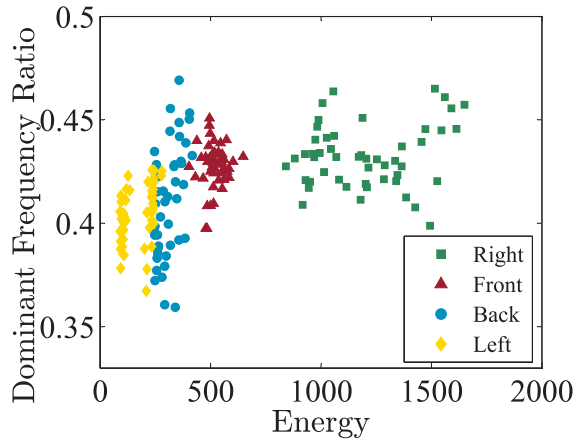


Fig. 8. Frequency domain analysis provides useful clues for posture classification. Energy and Dominant frequency ratio from the frequency domain features are selected as the example features.

Table II. Standard Deviation of Filtered RSS at Different Postures

Postures	Standard deviation
Front	1.4168
Right	1.9392
Left	0.5908
Back	1.2991

In the first type, a human's oro-nasal airflow is obstructed and there is no breathing related movements in the lungs and chest muscles. In central apnea, this stoppage of breathing occurs for more than 10 seconds [Berry et al. 2012]. In the second type, the intensity of breathing motion and movement of chest muscles is substantially low. In hypopnea, such low intensity breathing happens for more than 10 seconds [Berry et al. 2012]. Although there are other types of apnea such as obstructive apnea, mixed apnea, and the like, the two types of changes in breathing pattern (stoppage or low intensity) are commonly associated with them. Hence, we primarily focus on central apnea and hypopnea. Our intuition behind this investigation is that during both apnea events, the motion of chest muscles is significantly different. If so, it is possible to detect the apnea events using mmVital monitoring system. Since apnea is an abnormal breathing pattern, the frequency filter that extracts the breathing rate is not required. Instead, we can monitor the flatness or the shallow variations on the denoised RSS samples to detect the apnea events.

Utilizing mmWave for monitoring apnea events has an added advantage that its time-series RSS samples are already a good representation of human chest motion. This means that with only denoising and the filtering process (mentioned in Section 3.3), the apnea event can be detected in real time.

Examples of filtered RSS samples with two types of apnea events are shown in Figure 9. We use NeuLog respiration monitor (chest strap) [NeuLog 2015] to establish the ground truth of apnea events. Figure 9 demonstrates that the processed mmWave RSS samples provide clear indications of apnea (similar to polysomnography tests). The central apnea is detected when the distance between two peaks is (or absence of any peak for) more than 10 seconds. The hypopnea events are detected by measuring the amplitude of the reflected RSS. If the amplitude drops below 30% of normal breaths for more than 10 seconds [Berry et al. 2012], a hypopnea event is detected.

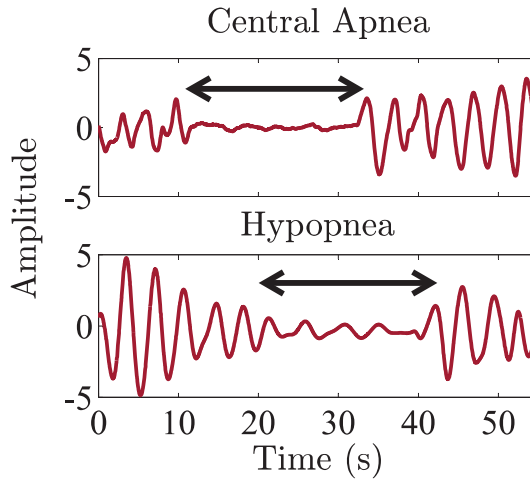


Fig. 9. Examples of central apnea and hypopnea events as observed through RSS variations.

6. FINDING HUMAN FOR VITAL SIGN MONITORING

A major challenge in the design of mmVital is that it is required to determine where the human is before it can start monitoring his/her vital signs. In home, office, or a similar indoor place where humans can freely move from one place to another, mmVital should be able to *find* the human and point the transmitted signal toward his/her body.

In this section, we introduce a *human finding* procedure that can be used to determine precise Tx and Rx angles to transmit the signal to a human body and receive the reflection, respectively. The challenge of human finding is further complicated by the fact that a 60GHz signal is reflected by many different objects in an indoor environment. Such objects include walls, metal objects such as cupboards, monitors, microwave, trash-cans, and so on. In the presence of many possible reflections, it is difficult for the Tx and Rx to know which reflection is indeed coming from a human.

mmVital utilizes a novel approach to distinguish humans from objects based on reflective loss as it is known to be different for different objects [Langen et al. 1994].

The permittivity dictates the amount of signal that penetrates the object and reflects from it. Apart from penetration and reflection, the signal is also absorbed by the objects and scattered from its surface. However, absorption and scattering effects are difficult to measure in our system. Instead, mmVital leverages the difference in reflection loss due to the different permittivity to distinguish the objects from a human.

In order to measure the reflection loss, it is first necessary to remove the effect of distance dependent path loss. Figure 10(a) shows an example reflection event from an object. If transmission power is P_T , transmit antenna gain is G_T , received power is P_R , and receiver antenna gain is G_R , the total loss $L = (P_T + G_T + G_R) - P_R$ is as follows

$$L = L_P(d_T) + L_P(d_R) + L_R(\epsilon_o), \quad (6)$$

where $L_R(\epsilon_o)$ is reflection loss from an object with permittivity of ϵ_o , and d_T and d_R are the distances of the object from the Tx and Rx, respectively. The reflection loss can be calculated as shown in Section 4.2. The path loss $L_P(d_T)$ and $L_P(d_R)$ at distance d can be calculated using the Friis model of free-space attenuation as

$$L_P(d_T) = 20 \log_{10} \left(\frac{4\pi d_T}{\lambda} \right) \quad (7)$$

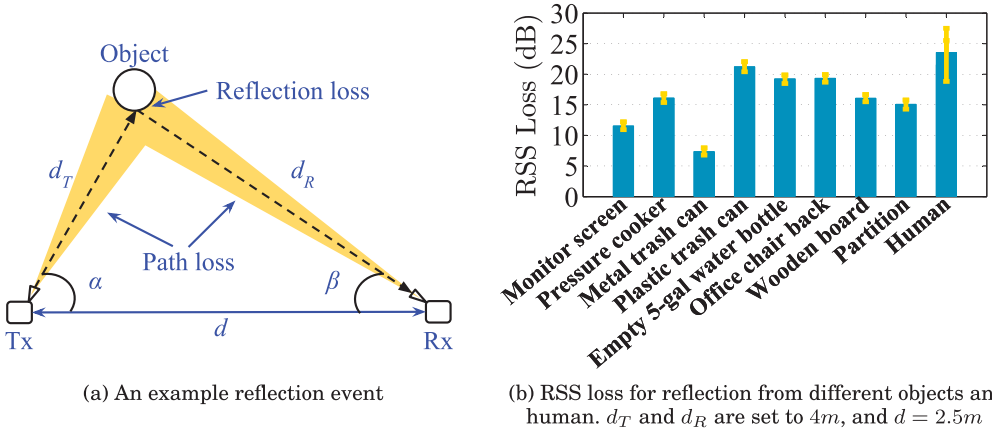


Fig. 10. Reflection loss for different types of objects.

$$L_P(d_R) = 20 \log_{10} \left(\frac{4\pi d_R}{\lambda} \right), \quad (8)$$

where λ is the signal wavelength. The Tx and Rx have the knowledge of P_T and P_R , and the distance between them (d). As shown in Figure 10(a), d_T and d_R can be calculated using the angle of transmission (α) and reception (β) to derive $L_P(d_T)$ and $L_P(d_R)$. Using Equations (6), (7), and (8), they can calculate the reflection loss $L_R(\epsilon_o)$. The reflection loss can then be used to distinguish if the reflection is coming from a human or an object.

To evaluate the feasibility of the object/human classification based on reflection loss, we test a variety of reflective objects and place them at one fixed location (fixed path loss) one by one. The observed RSS values for the objects and human, we are shown in Figure 10(b). Based on a 30-second measurement for each target, we can observe that different objects and humans, depending on their material permittivity, reflects different amounts of signals. Hence, we use regression on the reflection loss to identify if it is from an object or a human. In our experiments, we observe that the human/object classification can be done using even a single RSS sample based on the reflection loss, making the human finding procedure very efficient. With the use of more RSS samples, the confidence of classification can be further improved since the RSS for human reflected signal varies more due to heartbeat and breathing motion compared to the objects.

Before the classification can be applied, mmVital is required to find the reflection profile of the indoor environment. The reflection profile can be found by a brute-force omni-directional sweeping of Tx and Rx beams. The procedure is formally described in Algorithm 1. For each Rx angle (in steps from 0° to 360°), the Tx scans the entire 360° to determine all reflections. Note that although the omni-sweep procedure is brute-force, it can be completed in a short time with digital beamforming where beam switching can be performed at much smaller time scales. Also, the procedure is only required to be performed when human's vital signs can no longer be monitored and the human finding procedure has to be initiated. Also, both Tx and Rx can use discrete steps for angle increment for generating non-overlapped beams (similar to sectors in 802.11ad) to reduce the time complexity.

To demonstrate the omni-sweep procedure, we use our testbed to build the reflection profile of a room. Due to our horn antenna 3-dB beamwidth of 12° , the Rx scans all directions in increments of 12° . For each Rx angle, Tx scans the entire 360° with

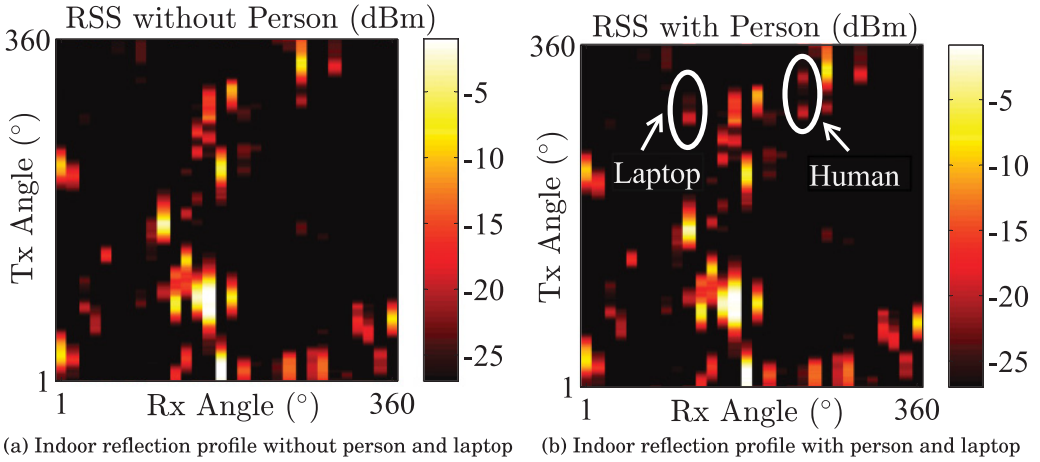


Fig. 11. Changes in the reflection profile can be monitored to detect new reflections and to determine if the new reflection is from a human or an object.

ALGORITHM 1: Human Finding Procedure

Input: Tx power (P_T), RSS variation tolerance threshold (κ), Beam sweep step size (s°), number of previous RSS samples (k), Human/object classifier ($\Psi(\cdot)$), distance between Tx and Rx (d)

Output: Tx and Rx angles toward human

Procedure:

```

1: for  $\alpha : 0^\circ \rightarrow 360^\circ$  do                                     #Omni-sweep procedure
2:   for  $\beta : 0^\circ \rightarrow 360^\circ$  do
3:      $R_{(\alpha,\beta)}^t = \text{RSS}(\alpha, \beta)$ 
4:      $\Delta_{(\alpha,\beta)}^t = |R_{(\alpha,\beta)}^{t-1} - R_{(\alpha,\beta)}^t|$ 
5:     if  $\Delta_{(\alpha,\beta)}^t > \kappa$  then                               #Change in reflection
6:       Calculate  $d_T$  and  $d_R$  using  $\alpha, \beta$  and  $d$ 
7:       for  $i : t - k \rightarrow t$  do                               #Analyze last  $k$  samples
8:          $L_{(\alpha,\beta)}^i = P_T - R_{(\alpha,\beta)}^i - L_P(d_T) - L_P(d_R)$ 
9:          $\Gamma_{(\alpha,\beta)} = \Gamma_{(\alpha,\beta)} \cup L_{(\alpha,\beta)}^i$ 
10:      end for
11:      if  $\Psi(\Gamma_{(\alpha,\beta)}) = \text{"Human"}$  then                   #Human-object
12:        return  $\alpha, \beta$                                      #classification
13:      end if
14:    end if
15:     $\beta = \beta + s^\circ$ 
16:  end for
17:   $\alpha = \alpha + s^\circ$ 
18: end for

```

continuous rotation. The reflection profile in the absence of any human is shown in Figure 11(a). As we can see, a typical room has many different reflections from walls and other objects. In mmVital, the profile can be built in the absence of a human and then only the changes in reflections need to be monitored to find a human. Note that a change in reflection can occur due to the presence of a human (increase if new reflection

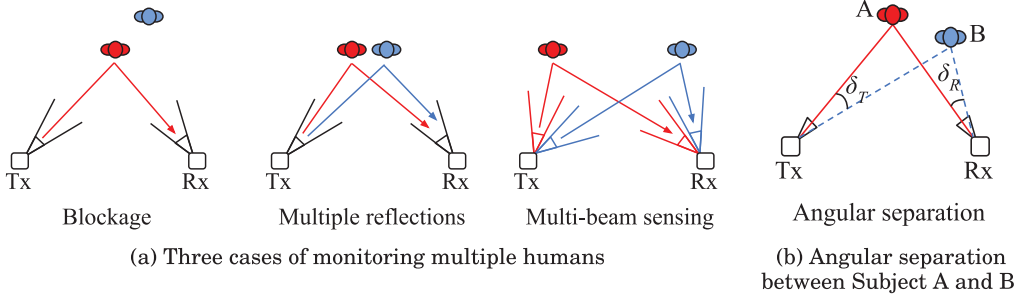


Fig. 12. (a) Relative position of humans compared to Tx and Rx gives rise to three cases - blockage, multiple reflections, and multi-beam sensing. (b) Angular separation between two humans can be calculated as $\min(\delta_T, \delta_R)$.

and possible decrease if existing reflection blocked) as well as movement of any existing object (e.g., moving a chair or laptop). Figure 11(b) shows the reflection profile with a human and a laptop (with metal enclosure) in the room. Both laptop and human reflect the signal, which can be tagged as the change in the reflections. As in Algorithm 1, each change in reflection is inspected using the reflection-loss-based classifier to identify if the change is due to a human or an object.

As we observe from Figure 11(b), in some cases, the existing reflections exhibit minor differences in RSS at different times. This can be due to the changes in object temperature. In order to ignore such minor variations, we utilize an RSS variation tolerance threshold (κ). Whenever a change in RSS is within the threshold, mmVital does not consider the reflection for object-human classification. Lastly, for the changed reflections, the Tx and Rx angles are used to determine the path loss and calculate the reflection loss as in Equation (6). This reflection loss is input to the object-human classifier, and if the reflection loss is classified as “human,” the Tx and Rx angles of the reflections are used to start monitoring the human for his/her vital signs.

7. MONITORING MULTIPLE HUMANS

Due to the directional nature of 60GHz communication, it can monitor multiple humans in a room concurrently. Monitoring multiple humans is useful in many practical scenarios. For example, more than one family member in a house or multiple patients in a hospital room can be monitored in parallel using the same mmWave Tx-Rx pair. In this section, we first systematically categorize various scenarios of monitoring multiple people with mmWave and then study how much separation between humans is necessary to sense their vital signs in parallel.

7.1. Single and Multi-Beam Sensing

The cases of monitoring multiple humans can be classified as follows (refer to Figure 12(a))—

- (1) **Single-Beam Sensing:** In single-beam sensing, two (or more) humans are monitored with the use of only one pair of fixed Tx and Rx beams without any switching of beam direction. These cases can be further classified into two classes:
 - (a) *Blockage* where one human blocks the other human completely, allowing only one human to be monitored at a time.
 - (b) *Multiple reflections* where mmWave signal is reflected partially from both the humans. With multiple reflections, it is possible to sense the vital signs for both the humans if they have distinct heart and breathing rates. Most of the current 2.4/5GHz RF-based vital sign monitoring research [Liu et al. 2015;

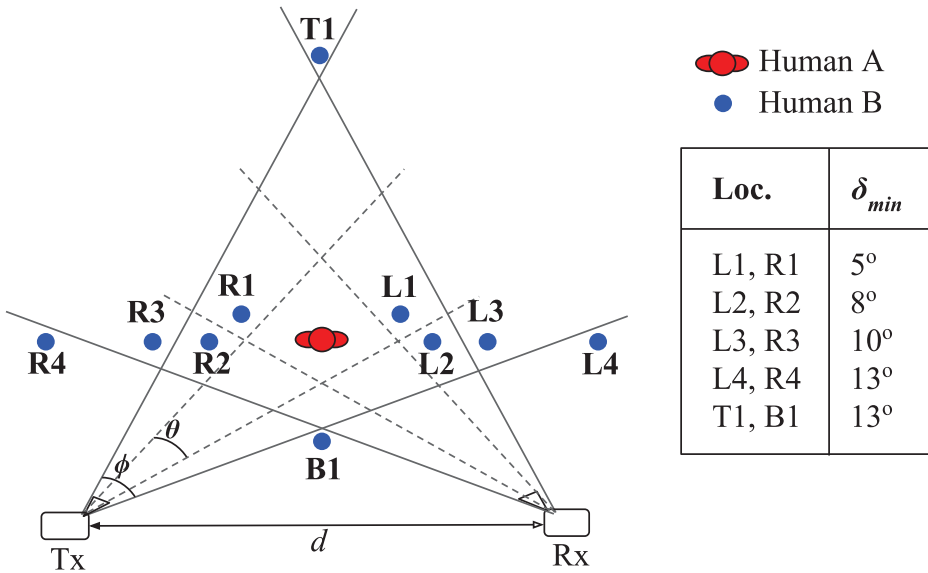


Fig. 13. Experiment setup used for evaluating the impact of angular separation.

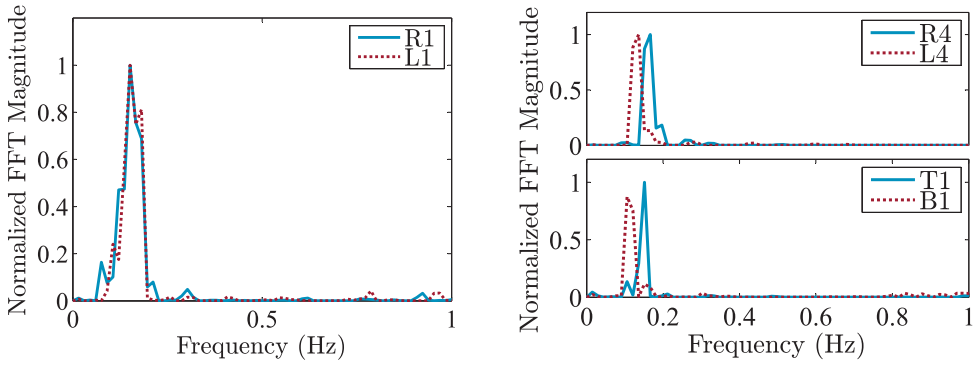
Ravichandran et al. 2015; Abdelnasser et al. 2015] assume such distinct vital signs of users for all users within the omni-directional range of the Tx and Rx. However, in reality, multiple users can have similar vital signs and even the vital signs vary substantially over time. With mmVital, such restrictions of distinct vital signs are limited only to a small region within the beams.

- (2) **Multi-Beam Sensing:** When there is a second human outside the Tx and Rx beams of the first human being monitored, both of them can be monitored by switching the beams between the two at a fast rate (using digital beamforming in nanoseconds [Valdes-Garcia et al. 2010]). We refer to such cases as *multibeam monitoring* (Figure 12(a)), where multiple non-interfering beams are used by the Tx and Rx to monitor people outside the beams of each other.

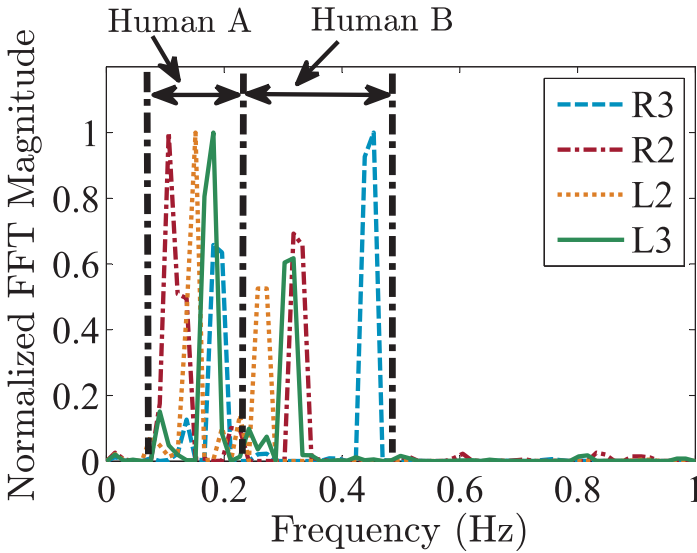
7.2. Human Separation

We now study the separation necessary between two humans for all cases of single and multi-beam sensing. In order to characterize the spatial reuse (from sensing perspective) in the area of interest, we identify two types of separation—angular and distance. As shown in Figure 12(b), let δ_T denote the angle between the straight lines connecting Tx to human A and human B. Similarly, let δ_R denote the angle between the straight lines connecting Rx to human A and human B. The *angular separation* (δ_{min}) is defined as $\min(\delta_T, \delta_R)$. The *distance separation* (s) is simply calculated as the Euclidean distance between human A and human B.

7.2.1. Angular Separation. We now empirically derive a relationship between the minimum required angular separation and the antenna beamwidth. In our experiment setup (Figure 13), one human (A) stands in the center with Tx and Rx pointing their beam to him/her. Another human (B) changes his/her position from L_1 to L_4 and R_1 to R_4 to vary the angular separation from 5° to 13° . Recall that in our testbed, the FNBW $\phi \approx 24^\circ$ and 3-dB beamwidth $\theta = 12^\circ$. We intentionally ask humans A and B to breathe at different rates (human A at 8–11Bpm and human B at 21–27Bpm) in order to make



(a) FFT of RSS samples for subject A when subject B is at locations R1 or L1 (blockage) (b) FFT of RSS samples for subject A when subject B is at locations R4, L4, T1 or B1 (multi-beam sensing)



(c) FFT of RSS samples for subject A when subject B is at locations R3, R2, L2, or L3 (multiple reflections)

Fig. 14. FFT of RSS samples for subject A when subject B stands at different locations (Figure 13) to create blockage, multiple reflections and multi-beam sensing scenarios.

their breathing rates distinguishable in the frequency domain. We repeat the setup and experiments in three different rooms for verification.

Figures 14(a), 14(b), and 14(c) show normalized FFT of the received RSS for the 10 cases. We choose locations L_1 and R_1 to emulate blockage scenarios where either the signal is blocked by human A before it reaches human B (L_1) or the signal reflection from human B (R_1) is blocked by human A before it reaches the receiver. We observe from Figure 14(a) that for Locations L_1 and R_1 of human B, only human A's breathing can be detected from the reflected RSS.

For locations L_2 , L_3 , R_2 , and R_3 , the transmitted signal is reflected from both humans A and B (multiple reflections). This can be seen as FFT peaks around 0.23–0.45Hz (human B) and 0.13–0.18Hz (human A) in Figure 14(c). It shows that vital signs of both humans can be calculated by applying appropriate frequency band-pass filters.

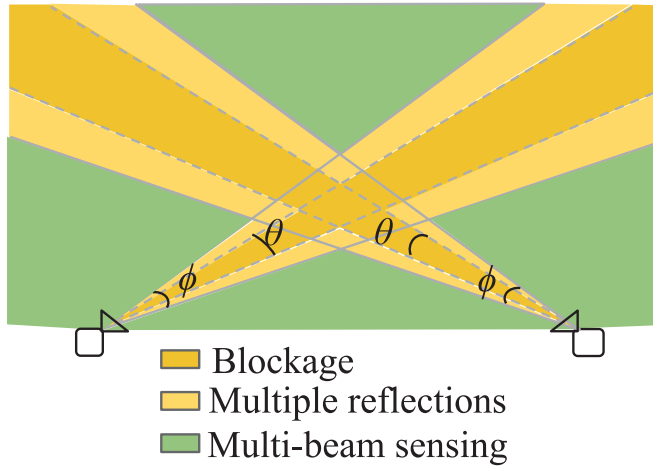


Fig. 15. Schematic showing physical regions of blockage, multiple reflections, and multi-beam sensing.

At locations L_4 , R_4 , T_1 , and B_1 , no breathing of human B is detected in Figure 14(b), indicating that human B is outside the Tx and Rx beams being used for human A. For these cases, both A and B can be monitored by switching the beams between them in time.

The following relationship between the angular separation and the beamwidth is observed from the above experiments. It is also schematically shown in Figure 15.

- (1) **Blockage:** when the angular separation between two humans is less than half the 3dB beamwidth of antenna $0 \leq \delta_{min} \leq \frac{\theta}{2}$, one human is likely to block the signal from impinging the other human.
- (2) **Multiple reflections:** when the angular separation between two humans is $\frac{\theta}{2} \leq \delta_{min} \leq \frac{\phi}{2}$, both humans can be monitored in parallel as long as their breathing/heart rates are different.
- (3) **Multi-beam sensing:** when $\delta_{min} > \frac{\phi}{2}$, both humans can be monitored by switching the beams between the two at a fast rate.

7.2.2. Distance Separation. The angular separation is essential to understand the conditions that dictate single and multi-beam sensing cases. However, it does not provide sufficient insight in how much physical distance is required between two humans for parallel sensing. In this section, we study distance separation and derive its relationship with beamwidth and relative positioning of Tx, Rx, and human subjects.

Figure 16 shows an example setup where the Tx and Rx pair is monitoring a human at location O. Let $\alpha = \angle OAB$ and $\beta = \angle OBA$ indicate the Tx and Rx beam directions, respectively. We assume that Tx is located at Point $A(-d/2, 0)$ and Rx is located at Point $B(d/2, 0)$ where d is the distance between Tx and Rx. We can observe from Figure 13 that another human can be at the four nearest locations (points $C(x_C, y_C)$, $D(x_D, y_D)$, $E(x_E, y_E)$, and $F(x_F, y_F)$ in Figure 16) for multi-beam sensing. Here, we primarily focus on the multi-beam sensing cases as they are more practical compared to multiple reflection cases which occur in relatively smaller areas and also require the users' vital signs to be different. We define the distance separation (s) to be the minimum of the four distances OC , OD , OE , and OF . The distance s indicates the best-case of minimum separation necessary between the two humans. It is dependent on α , β , and ϕ (FNBW), and can occur in any direction from the human at location O.

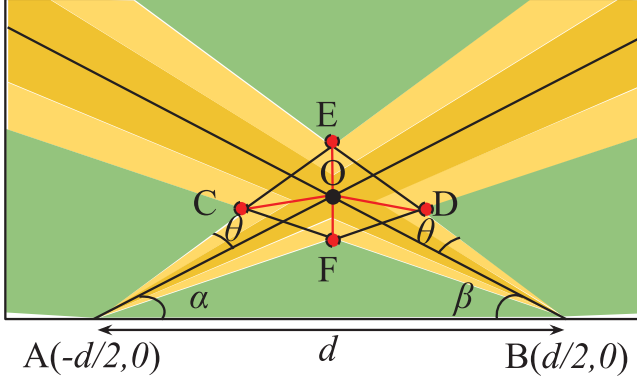


Fig. 16. Four nearest locations where another human can be present without interfering with the target human at Point O .

The four distances OC , OD , OE , and OF can be calculated by deriving the coordinates of the points in the 2D Euclidean space. Note that we assume $\theta = \frac{\phi}{2}$ because the 3dB beamwidth can be approximated as half of FNBW in most mmWave horn antennas. Using these, X and Y coordinates of Point O (when $\theta < \alpha$, $\theta < \beta$) can be calculated as

$$x_o = \frac{-d}{2} + \frac{d \cos \alpha \sin \beta}{\sin(\alpha + \beta)}; y_o = \frac{d \sin \alpha \sin \beta}{\sin(\alpha + \beta)}. \quad (9)$$

The complete derivation of the coordinates of points and four distances can be found in Yang et al. [2016b]. We use them to calculate the best-case distance separation (s^*).

In the experiment setup of Figure 13, we also evaluate two additional locations (T_1 and B_1) for human B. As we observe from Figure 14(b), we observe that the presence of human B is not detected in the FFT which means that it has a sufficient distance separation from human A to allow multi-beam sensing. We also evaluate the best-case distance separation for all points in a room of $10\text{m} \times 10\text{m}$ and the results are shown in Figure 17. We find that for the majority of locations within the room, the value of s^* is relatively small (median = 1.67 meters) which indicates that mmVital in our testbed setup can monitor multiple humans even when they are relatively close to each other.

8. EVALUATION

We perform an extensive evaluation of mmVital in two different indoor scenarios as shown in Figure 18. The first room is a laboratory room (size: $6\text{m} \times 9\text{m}$) in a university building with objects such as cubicle partitions, white boards, metal cupboard, computers, and the like. The second room is an apartment bedroom of size $4.5\text{m} \times 6\text{m}$ with a bed in the center and other furniture on the sides. Figure 18 shows the positions of Tx and Rx. The transmission power is set to 0dBm and the horn antenna is 24dBi, both of which are under the regulation at 60GHz frequency [Rappaport et al. 2014]. Power density is a commonly used metric to evaluate the amount of power exposed to a human body. The power density (P_D) can be calculated as

$$P_D = \frac{P_T G_T}{4 \cdot \pi \cdot d_T^2}, \quad (10)$$

where P_T and G_T denote transmission power and the gain of antenna, respectively; d_T denotes the distance between the object and the transmitter in meters. This indicates that even though the human is very close to the transmitter (at 0.1m), the observed

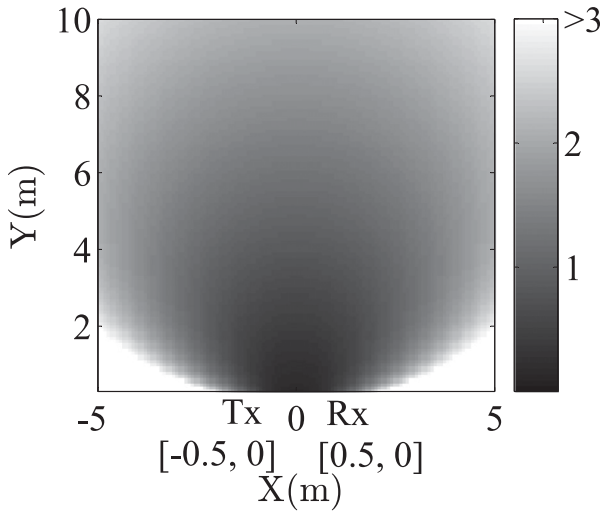


Fig. 17. Best case distance separation in a $10m \times 10m$ room.

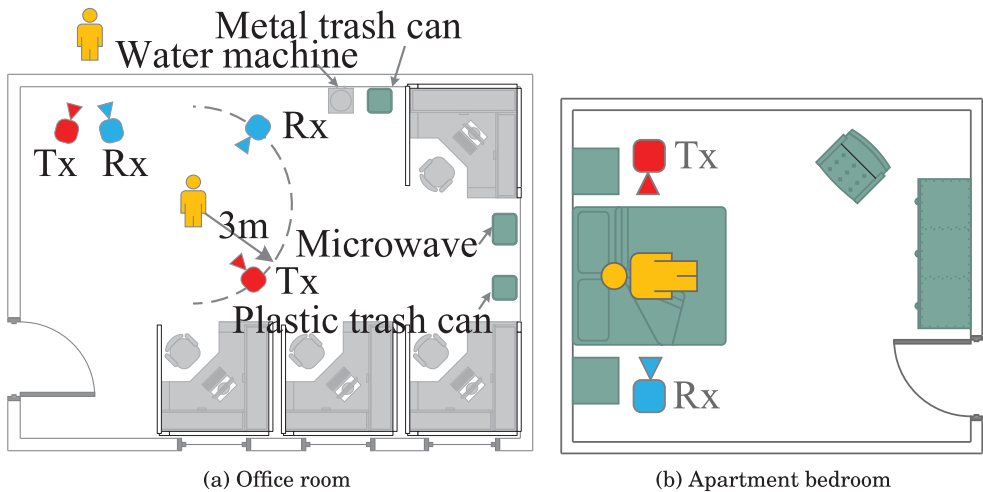


Fig. 18. Experiment setup in office and home.

power density is $191mW/m^2$, which is still significantly lower than the maximum allowable value of $200W/m^2$ at $30GHz \sim 300GHz$ as per the ANSI/IEEE C95.1-2005 standard [Wu et al. 2015]. We enroll seven participants over a period of two weeks to monitor their vital signs. Out of the seven subjects, six subjects have a Body Mass Index (BMI) of around $19-25kg/m^2$ and one subject (Subject #6) has the BMI of around $29kg/m^2$. The BMI is correlated with breathing rate and other cardiovascular parameters [Sorlien 2015]. Table III shows the detailed information of subjects. In our experiments, all human subjects were wearing ordinary casual clothes. Different type of clothing/fabric can be worn by people in their daily lives. Also, it is likely that a patient can be under sheets/blankets while sleep monitoring is carried out. Measurement studies such as in the work of Bjarnason et al. [2004] and Xiao et al. [2008] show that common fabric materials (such as cotton, linen, and wool) do not significantly

Table III. Gender, Height, Weight, and BMI Information of Seven Subjects

Subject Index	Gender	Height (cm)	Weight (kg)	BMI
# 1	M	168.2	65.1	23.2
# 2	M	180.7	79.8	24.4
# 3	F	170.5	61.6	21.2
# 4	M	172.1	65.3	22.0
# 5	F	163.3	50.5	18.9
# 6	M	169.1	84.1	29.4
# 7	M	168.0	72.4	25.7

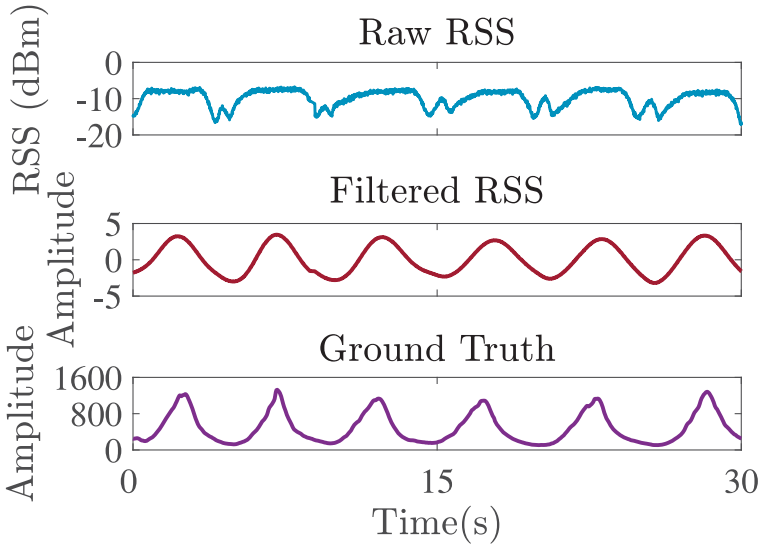


Fig. 19. An example of raw RSS, filtered RSS, and ground truth on monitoring breathing rate.

attenuate the millimeter wave signal even in case of multiple layers of bed coverings or pull-overs. However, in this work, we focus on experimentation with people wearing normal clothing to evaluate our system.

The ground truth is established using a finger pulse oximeter [Gurin 2015] (for heart rate) and Neulog chest-strap respiration monitor [NeuLog 2015]. Note that the finger pulse oximeter is only able to provide a numeric value of heart beats. On the other hand, the wearable breathing rate monitor records the complete breathing signal as shown in Figure 19. Based on the ground truth, the mean estimation error is defined as

$$\text{Mean estimation error} = \frac{\sum_{i=1}^m |\text{ground truth} - \text{estimated vital sign}|}{m}, \quad (11)$$

where m denotes the duration of measurement in minutes, and ground truth and estimated vital signs are measured in bpm (heart rate) or Bpm (breathing rate).

8.1. Accuracy of Vital Sign Monitoring

8.1.1. Breathing and Heart Rate Estimation Accuracy. For evaluating the breathing and heart rates of participants, we use three different incident angles in the university room. Figure 20(a) and (b) show the mean estimation error with (95% confidence internals) for breathing rate (Bpm) and heart rate (bpm) for the seven participants at three different incident angles (70° , 50° , 30°). The accuracy is calculated for three

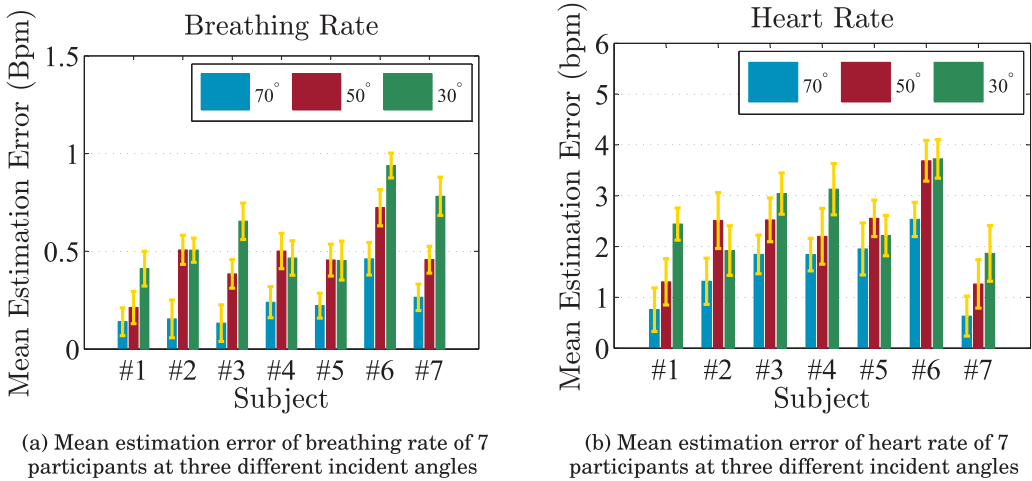


Fig. 20. Accuracy of breathing rate and heart rate.

experiment runs of 10 minutes for each of the participants. For the incident angle of 70° , the mean estimation error in breathing rate and heart rate estimation is less than 0.5Bpm and 2.5bpm, respectively, for all seven participants. This shows that 60GHz vital sign monitoring can provide a highly reliable estimate of breathing and heart rates. The estimation error increases with the decrease in the incident angles, which proves the relationship between the reflection loss and the incident angle discussed in Section 4.2. At higher incident angles, the reflection loss decreases as well as the reflected RSS is observed to be less noisy. Both these factors increase the vital sign estimation accuracy. We observe that the breathing and heart rate estimation errors are slightly higher for Subject #6, which is likely due to higher BMI. Since these experiments are performed with the participants either standing or sitting, the estimation error is likely to be even lower when they are sleeping on a bed as one's breathing rate is substantially more stable when a human is sleeping.

8.1.2. Robustness to Distance and Posture. We also evaluate the impact of a human's distance from Tx and Rx on the observed RSS and the accuracy of vital sign monitoring. We fix the incident angle to be 45° and the location of the human subject, while moving the Tx and Rx away from the human in steps of 1 meter. We evaluate the RSS and breathing rate estimation accuracy while varying the Tx-human (and Rx-human) distance from 1 meter to 10 meters. Figure 21(a) shows RSS loss and breathing rate estimation accuracy for the varying distance. Note that the distance in Figure 21(a) indicates the Tx to human (or human to Rx) distance, so the total signal propagation distance (Tx to human and human to Rx) is actually double. As expected, the RSS loss increases and estimation accuracy decreases with increase in distance. The confidence intervals on RSS loss indicates that sufficient variations in the signal is observed even at a larger distances (up to a Tx-human distance of 8 meters). Recall that this signal variation is useful in finding the human and distinguishing its reflection from other objects (Section 6). For distances lower than 8 meters, the mean breathing rate estimation error is less than 0.42Bpm (mean accuracy is 98.8%), and beyond 8 meters the mean estimation error drops close to 1.07Bpm, (mean accuracy is 97%). This shows that the vital sign estimation of mmVital is robust to distances common in rooms of typical indoor spaces like offices and homes.

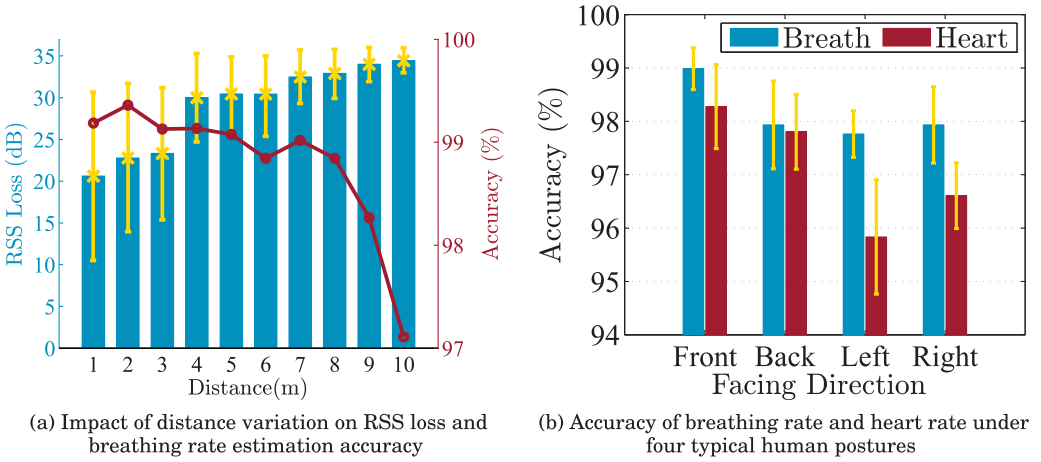


Fig. 21. Impact of distance apart, and robustness to different postures.

Since the signal can impinge anywhere on the human body depending on the human's orientation relative to the Tx and Rx, we evaluate the impact of a human's facing direction (or posture) on breathing and heart rate estimation accuracy. In this experiment, five participants are asked to lay down and pretend to sleep on the bed in the apartment bedroom (see Figure 18(b)) for 3 minutes (repeated 10 times) in four different postures: sleeping on back (Front), sleeping on stomach (Back), facing left (Left) or facing right (Right). The antenna height of Tx and Rx is set as 1.2m. The results of breathing rate and heart rate estimation accuracy are shown in Figure 21(b). We observe that the highest breathing rate estimation accuracy is observed for the front posture in which the signal directly strikes and reflects from a human's chest area, which exhibits the maximum breathing motion. However, for the other three postures, breathing rate estimation accuracy also remains close to 98%. In terms of heart rate estimation, front posture also provides highest accuracy, followed by the back posture. In both front and back postures, the reflected signal better captures the heart beat motion compared to left and right postures. When the human is facing right, his/her heart is toward the incoming signal from the Tx compared to when she is facing left, resulting in a better heart rate estimation accuracy for the right posture. In all cases, we observe that mmVital achieves high vital sign monitoring accuracy even when the human is in different postures.

8.1.3. Behind a Wall Estimation. The breathing rate estimation accuracy is evaluated for the behind-the-wall case shown in Figure 18(a). Here, a human stands on the other side of the wall from the Tx-Rx pair. Because penetration loss and reflection loss change depending on the incident angle, two incident angles (10° , 20°) are evaluated. The mean estimation error of breathing rate is observed to be 0.58Bpm and 0.93Bpm for 10° and 20° , respectively. In contrast to line-of-sight cases, an increase in incident angle increases the estimation error in behind-the-wall cases. This is because at higher incident angles, more signal is reflected and a lesser signal penetrates through the wall to strike a human body. The RSS reflected also undergoes the same phenomenon and the received RSS carries a weaker signature of breathing motion. It is worth noting that if the application does not require behind-the-wall monitoring, the transmission power can be reduced or larger incident angles can be used (more reflection, less penetration) to contain the 60GHz signal within the room.

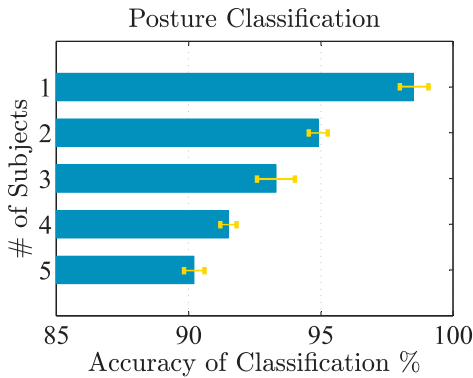


Fig. 22. Accuracy of posture classification for five subjects. Number (#) of subjects refers to how many subjects are involved in the training and testing.

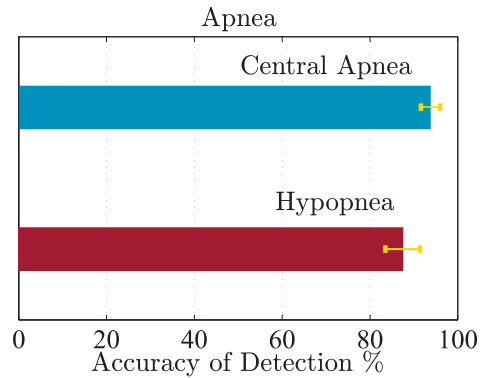


Fig. 23. Accuracy of central apnea and hypopnea detection.

8.2. Posture Classification and Apnea Detection

We evaluate our posture detection and classification and apnea detection schemes with five participants sleeping in an apartment bedroom scenario (Figure 18(b)). For the posture detection, the detection scheme in Section 5.1 is applied on the time duration in which each participant is asked to make 100 random posture changes. The variance-based posture change detection scheme achieves a very high accuracy of 99.6%.

For the posture classification, we use the machine learning classifier described in Section 5.1 using the data from a varying number of participants. For each participant, we evaluate 40 instances of four postures (a total of 160 for one participant). The results of posture classification accuracy are provided in Figure 22. Ten-fold cross-validation is used to evaluate the machine learning classifier. The results show that when trained and tested for the same participant (the number of subjects is one), the average posture classification accuracy is higher than 98%. For a classifier built using the data of all five participants (the number of subjects is five), the posture classification accuracy is higher than 90%. The reduction in classification accuracy with more subjects can be attributed to how different people assume the postures and BMI variations. It is also observed that the majority (over 89% of misclassified instances) of misclassification occurs between “back” and “facing left” postures.

Figure 23 shows the apnea event detection accuracy for central apnea and hypopnea. For the apnea experiments, participants emulate the apnea events while lying on the bed in different postures. We evaluate 16 central apnea and 16 hypopnea events using the technique described in Section 5.2. The detection accuracy of central apnea and hypopnea is observed to be 93.7% and 87.5%, respectively. The lower detection accuracy of hypopnea is mostly due to the fact that during the emulated events, different participants drop the breathing intensity at different levels (not necessarily 30%), making it difficult to set the detection threshold, which in turn results in the unsuccessful detection of some events.

8.3. Reflection Loss-based Human Finding

The human finding procedure described in Algorithm 1 is evaluated in the laboratory room scenario. We create 20 different scenarios where eight objects (laptop, metal kitchen utensil, plastic trash can, metal trash can, empty 5gal. water bottle, chair, wooden board, partition board) and a human subject are randomly relocated inside the room. Similarly, Tx and Rx are also moved to randomly chosen points in the room.

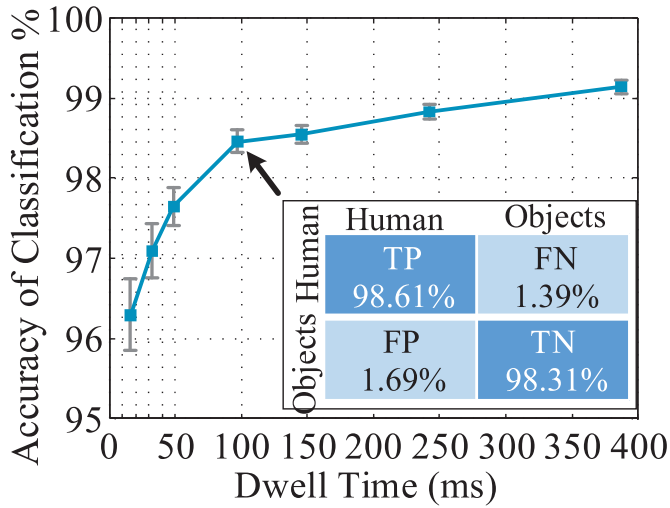


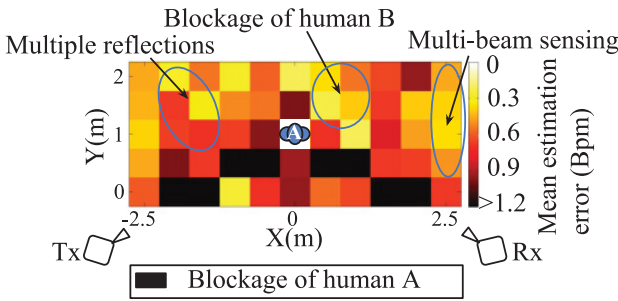
Fig. 24. Accuracy of object/human classification with varying dwell time (number of RSS samples). TP, FN, FP, and TN denote true positive, false negative, false positive, and true negative, respectively.

The movement of objects, human, and Tx-Rx ensures that a wide variety of distances and incident angles are evaluated for moving as well as non-moving objects (walls, tables, etc.). For each of the 20 scenarios, we find the reflection profile to determine the reflection from moved objects and the human. The reflection loss-based classification is then applied to the RSS values of changed reflections as described in Section 6. The results of the classification are presented in Figure 24. We vary the time interval for which RSS samples are collected (dwell time) at each angle before performing the classification. It can be observed that as the dwell time increases, the accuracy of human-object classification increases. Whether a reflection is from a human or an object can be determined with an average accuracy of 96.2% only with one RSS sample (available after 16ms). With 100ms of dwell time, the accuracy increases to 98.4% with false-positive rate of <2%. This means that the human finding procedure is highly robust to environment changes and can accurately determine the Tx and Rx angles for monitoring.

8.4. Monitoring Vital Signs of Multiple People

To evaluate the accuracy of vital sign estimation for multiple people using mmVital, we carefully design an experiment as shown in Figure 25(a) and 25(b). In this setup, we choose a rectangular area of 6m × 2.5m in which human subject A stands at the center of the rectangle. The Tx and Rx point their antenna beams toward human A. We then ask human B to stand at different 0.5m × 0.5m square blocks within the rectangle. In order to create and detect all of the scenarios we proposed in Section 7, we ask both subjects to intentionally breathe at different rates. For each position of human B, we estimate the breathing rate of human A. Figure 25(a) shows a heat map where the color of each square block indicates human A's mean estimated breathing rate error, when human B is standing in the square. Note that human A's location remains unchanged during the experiment.

In Figure 12(a), the signal transmitted toward or reflected from human A is affected by the presence of human B at different positions, resulting in (1) blockage, (2) multiple reflections, and (3) multi-beam sensing cases as discussed in Section 7. For the case that human B is between Tx and human A (the black blocks), the transmitted signal does not



(a) Heat map showing the mean estimation error of human A's breathing rate when human B is standing at different square blocks



(b) Experiment setup with different separations between two humans

Fig. 25. Accuracy of human finding and multiple people.

reach human A, resulting in blockage of human A. When human B is close to human A, the transmitted signal is reflected from both the humans (multiple reflections). However, due to the presence of human B, the mean estimation error of the breathing rate of human A drops close to 0.9Bpm (four adjacent positions of human A). For many locations when human B is sufficiently far from human A, it does not interfere with the vital sign monitoring (multi-beam sensing). This means that human B is outside the current Tx and Rx beam of human A (angular separation higher than half of the FNBW), and multiple separate Tx-Rx beam pairs can be used to monitor both humans. Due to the unavailability of digital beamforming phased array antenna for 60GHz, we leave the evaluation of multiple humans through fast switching Tx-Rx beams to future work.

9. CONCLUSIONS

In this article, we presented mmVital, a vital sign monitoring system utilizing mmWave signal reflected from the human body. We (1) empirically demonstrated the feasibility of the monitoring of breathing and heart rates using 60GHz mmWave signals; (2) developed a contactless sleep monitoring procedure that does not require the user to attach any devices on his/her body during sleep; (3) proposed a novel *human finding* technique that can locate a human body before vital sign monitoring using reflection loss characteristics. We extensively evaluated mmVital using a state-of-the-art 60GHz testbed and seven participants, and showed that it can provide accurate and robust (to incident angles and distances) vital sign monitoring, accurate posture change detection and classification, and timely central apnea and hypopnea detection. mmVital also investigates how to monitor multiple people concurrently in terms of angular and spacial separations. Monitoring multiple people is feasible due to directional nature of millimeter wave communication. mmVital is also shown to be effective in monitoring subjects behind a wall.

With the upcoming fifth-generation (5G) wireless networks, where millimeter wave technology will be widely used, our contribution can be implemented on the future millimeter wave WLAN devices that can serve as a communication as well as a sensing infrastructure. We note that our current evaluation of mmVital is limited to seven participants. As part of our future work, we plan to evaluate mmVital for a more diverse set of users with varying body and age characteristics. In our ongoing research, we are exploring human movement tracking through mmWave and other smart home applications.

REFERENCES

- Heba Abdelnasser, Khaled A. Harras, and Moustafa Youssef. 2015. UbiBreathe: A ubiquitous non-invasive WiFi-based breathing estimator. In *Proceedings of the 16th ACM International Symposium on Mobile Ad Hoc Networking and Computing*. ACM, 277–286.
- Fadel Adib, Hongzi Mao, Zachary Kabelac, Dina Katabi, and Robert C. Miller. 2015. Smart homes that monitor breathing and heart rate. In *Proceedings of the 33rd Annual ACM Conference on Human Factors in Computing Systems*. ACM, 837–846.
- Javad Ahmadi-Shokouh, Sima Noghianian, Ekram Hossain, Majid Ostadrahimi, and James Dietrich. 2009. Reflection coefficient measurement for house flooring materials at 57-64 GHz. In *Proceedings of the Global Telecommunications Conference (GLOBECOM'09)*. IEEE. IEEE, 1–6.
- S. Bakhtiari, T. W. Elmer, N. M. Cox, N. Gopalsami, A. C. Raptis, S. Liao, I. Mikhelson, and A.V. Sahakian. 2012. Compact millimeter-wave sensor for remote monitoring of vital signs. *IEEE Transactions on Instrumentation and Measurement* 61, 3 (March 2012), 830–841. DOI:<http://dx.doi.org/10.1109/TIM.2011.2171589>
- Richard B. Berry, Rohit Budhiraja, Daniel J. Gottlieb, David Gozal, Conrad Iber, Vishesh K. Kapur, Carole L. Marcus, Reena Mehra, Sairam Parthasarathy, Stuart F. Quan, and others. 2012. Rules for scoring respiratory events in sleep: Update of the 2007 AASM manual for the scoring of sleep and associated events. *J Clin Sleep Med* 8, 5 (2012), 597–619.
- J. E. Bjarnason, T. L. J. Chan, A. W. M. Lee, M. A. Celis, and E. R. Brown. 2004. Millimeter-wave, terahertz, and mid-infrared transmission through common clothing. *Applied Physics Letters* 85, 4 (2004), 519–521.
- Huey-Ru Chuang, Hsin-Chih Kuo, Fu-Ling Lin, Tzuen-Hsi Huang, Chi-Shin Kuo, and Ya-Wen Ou. 2012. 60-GHz millimeter-wave life detection system (MLDS) for noncontact human vital-signal monitoring. *IEEE Sensors Journal* 12, 3 (2012), 602–609.
- Fullpower. 2014. MotionX 24/7. Retrieved from <https://itunes.apple.com/us/app/motionx-24-7-sleeptracker/id505074676?mt=8>.
- S. Gabriel, R. W. Lau, and Camelia Gabriel. 1996. The dielectric properties of biological tissues: II. Measurements in the frequency range 10 Hz to 20 GHz. *Physics in Medicine and Biology* 41, 11 (1996), 2251.
- Om P. Gandhi and Abbas Riazi. 1986. Absorption of millimeter waves by human beings and its biological implications. *Microwave Theory and Techniques, IEEE Transactions on* 34, 2 (1986), 228–235.
- William F. Ganong and Kim E. Barrett. 2005. *Review of Medical Physiology*. Vol. 21. McGraw-Hill Medical, New York, New York.
- Gurin 2015. Finger Pulse Oximeters. Retrieved from <http://gurinproducts.com/products/oximeters/>.
- Ming-Chun Huang, Jason J. Liu, Wen Yao Xu, Changzhan Gu, Changzhi Li, and Majid Sarrafzadeh. 2016. A self-calibrating radar sensor system for measuring vital signs. *IEEE Transactions on Biomedical Circuits and Systems* 10, 2 (2016), 352–363.
- Hyeonseok Hwang, Joung-hwa Yim, Jei-Won Cho, Changyul Cheon, and Youngwoo Kwon. 2003. 110 GHz broadband measurement of permittivity on human epidermis using 1 mm coaxial probe. In *Proceedings of the 2003 IEEE MTT-S International Microwave Symposium Digest*, Vol. 1. IEEE, 399–402.
- IEEE. 2012. IEEE approved draft standard for LAN - specific requirements - part 11: Wireless LAN medium access control (MAC) and physical layer (PHY) specifications - amendment 3: Enhancements for very high throughput in the 60 GHz band. *IEEE P802.11ad/D9.0, July 2012 (Draft Amendment based on IEEE 802.11-2012)* (Oct 2012), 1–685.
- Intel. 2014. Intel Gigabit Wireless. Retrieved from <http://www.intel.com/content/dam/www/public/us/en/documents/product-briefs/tri-band-wireless-ac17265-brief.pdf>.
- Te-Yu Jason Kao and Jenshan Lin. 2013. Vital sign detection using 60-GHz Doppler radar system. In *Proceedings of the 2013 IEEE International Wireless Symposium (IWS)*. IEEE, 1–4.
- Hani A. Kayyali, Sarah Weimer, Craig Frederick, Christian Martin, Del Basa, Jesse A. Juguillon, and Felicitas Jugilioni. 2008. Remotely attended home monitoring of sleep disorders. *TELEMEDICINE and e-HEALTH* 14, 4 (2008), 371–374.
- B. Langen, G. Lober, and W. Herzig. 1994. Reflection and transmission behaviour of building materials at 60 GHz. In *Proceedings of the 5th IEEE International Symposium on Personal, Indoor and Mobile Radio Communications, 1994. Wireless Networks-Catching the Mobile Future*. IEEE, 505–509.
- Jian Liu, Yan Wang, Yingying Chen, Jie Yang, Xu Chen, and Jerry Cheng. 2015. Tracking vital signs during sleep leveraging off-the-shelf WiFi. In *Proceedings of the 16th ACM International Symposium on Mobile Ad Hoc Networking and Computing*. ACM, 267–276.
- David C. Mack, James T. Patrie, Paul M. Suratt, Robin A. Felder, and Majid Alwan. 2009. Development and preliminary validation of heart rate and breathing rate detection using a passive, ballistocardiography-

- based sleep monitoring system. *IEEE Transactions on Information Technology in Biomedicine* 13, 1 (2009), 111–120.
- A. Mamelak and J. A. Hobson. 1989. Nightcap: A home-based sleep monitoring system. *Sleep* 12, 2 (1989), 157–166.
- Juan F. Masa, Jaime Corral, Ricardo Pereira, Joaquin Duran-Cantolla, Marta Cabello, Luis Hernández-Blasco, Carmen Monasterio, Alberto Alonso, Eusebi Chiner, Manuela Rubio, and others. 2011. Effectiveness of home respiratory polygraphy for the diagnosis of sleep apnoea and hypopnoea syndrome. *Thorax* (2011), thx–2010.
- Ilya V. Mikhelson, Philip Lee, Sasan Bakhtiari, Thomas W. Elmer, Aggelos K. Katsaggelos, and Alan V. Sahakian. 2012. Noncontact millimeter-wave real-time detection and tracking of heart rate on an ambulatory subject. *IEEE Transactions on Information Technology in Biomedicine* 16, 5 (2012), 927–934.
- Emmanuel Munguia Tapia. 2008. *Using Machine Learning for Real-time Activity Recognition and Estimation of Energy Expenditure*. Ph.D. Dissertation. Massachusetts Institute of Technology.
- Rajalakshmi Nandakumar, Shyamnath Gollakota, and Nathaniel Watson. 2015. Contactless sleep apnea detection on smartphones. In *Proceedings of the 13th Annual International Conference on Mobile Systems, Applications, and Services*. ACM, 45–57.
- NeuLog 2015. NeuLog Sensors. Retrieved from <https://neulog.com/>.
- Anh Nguyen, Raghda Alqurashi, Zohreh Raghebi, Farnoush Banaei-kashani, Ann C. Halbower, Thang Dinh, and Tam Vu. 2016. In-ear biosignal recording system: A wearable for automatic whole-night sleep staging. In *Proceedings of the 2016 Workshop on Wearable Systems and Applications*. ACM, 19–24.
- Thomas Nitsche, Adriana B. Flores, Edward W. Knightly, and Joerg Widmer. 2015. Steering with eyes closed: Mm-wave beam steering without in-band measurement. In *Proceedings of the 2015 IEEE Conference on Computer Communications (INFOCOM)*. IEEE, 2416–2424.
- Mark B. Norman, Sally Middleton, Odette Erskine, Peter G. Middleton, John R. Wheatley, and Colin E. Sullivan. 2014. Validation of the Sonomat: A contactless monitoring system used for the diagnosis of sleep disordered breathing. *Sleep* 37, 9 (2014), 1477.
- Arie Oksenberg and Donald S. Silverberg. 1998. The effect of body posture on sleep-related breathing disorders: Facts and therapeutic implications. *Sleep Medicine Reviews* 2, 3 (1998), 139–162.
- Pasternack. 2015. Pasternack. Retrieved from <http://www.pasternack.com/60-ghz-test-development-system-pem003-kit-p.aspx>.
- Neal Patwari, Lara Brewer, Quinn Tate, Ossi Kaltiokallio, and Maurizio Bocca. 2014. Breathfinding: A wireless network that monitors and locates breathing in a home. *Selected Topics in Signal Processing, IEEE Journal of* 8, 1 (2014), 30–42.
- Douglas T. Petkie, Carla Benton, and Erik Bryan. 2009. Millimeter-wave radar for vital signs sensing. In *SPIE Defense, Security, and Sensing*. International Society for Optics and Photonics, 73080A–73080A.
- R. Prakash, Siva V. Girish, and A. Balaji Ganesh. 2016. Real-time remote monitoring of human vital signs using internet of things (IoT) and GSM connectivity. In *Proceedings of the International Conference on Soft Computing Systems*. Springer, 47–56.
- Jeffrey Price. 2012. *Practical Aviation Security: Predicting and Preventing Future Threats*. Butterworth-Heinemann.
- Theodore S. Rappaport, Robert W. Heath Jr, Robert C. Daniels, and James N. Murdock. 2014. *Millimeter Wave Wireless Communications*. Pearson Education.
- Ruth Ravichandran, Elliot Saba, Ke-Yu Chen, Mayank Goel, Sidhant Gupta, and Shwetak N. Patel. 2015. WiBreathe: Estimating respiration rate using wireless signals in natural settings in the home. In *Proceedings of the 2015 IEEE International Conference on Pervasive Computing and Communications (PerCom)*. IEEE, 131–139.
- Mahsan Rofouei, Mike Sinclair, Ray Bittner, Tom Blank, Nick Saw, Gerald DeJean, and Jeff Heffron. 2011. A non-invasive wearable neck-cuff system for real-time sleep monitoring. In *Proceedings of the 2011 International Conference on Body Sensor Networks*. IEEE, 156–161.
- Jae Hyuk Shin, Young Joon Chee, Do-Un Jeong, and Kwang Suk Park. 2010. Nonconstrained sleep monitoring system and algorithms using air-mattress with balancing tube method. *IEEE Transactions on Information Technology in Biomedicine* 14, 1 (2010), 147–156.
- Molly Sorlien. 2015. BMI and Respiratory Function. Retrieved from <http://www.livestrong.com/article/84685-bmi-respiratory-function/>.
- William H. Spriggs. 2014. *Essentials of Polysomnography*. Jones & Bartlett Publishers.
- Sanjib Sur, Vignesh Venkateswaran, Xinyu Zhang, and Parmesh Ramanathan. 2015. 60 GHz indoor networking through flexible beams: A link-level profiling. In *Proceedings of the 2015 ACM SIGMETRICS International Conference on Measurement and Modeling of Computer Systems (SIGMETRICS'15)*. ACM, New York, NY, USA, 71–84. DOI: <http://dx.doi.org/10.1145/2745844.2745858>

- Alberto Valdes-Garcia, Sean T. Nicolson, Jie-Wei Lai, Arun Natarajan, Ping-Yu Chen, Scott K. Reynolds, Jing-Hong Conan Zhan, Dong G. Kam, Duixian Liu, and Brian Floyd. 2010. A fully integrated 16-element phased-array transmitter in SiGe BiCMOS for 60-GHz communications. *IEEE Journal of Solid-State Circuits*, 45, 12 (2010), 2757–2773.
- Teng Wei and Xinyu Zhang. 2015. mtrack: High-precision passive tracking using millimeter wave radios. In *Proceedings of the 21st Annual International Conference on Mobile Computing and Networking*. ACM, 117–129.
- Ting Wu, Theodore S. Rappaport, and Christopher M. Collins. 2015. The human body and millimeter-wave wireless communication systems: Interactions and implications. In *Proceedings of the 2015 IEEE International Conference on Communications (ICC)*. IEEE, 2423–2429.
- Zelong Xiao, Jianzhong Xu, and Taiyang Hu. 2008. Research on the transmissivity of some clothing materials at millimeter-wave band. In *Proceedings of the International Conference on Microwave and Millimeter Wave Technology (ICMMT'08)*. Vol. 4. IEEE, 1750–1753.
- Zhicheng Yang, Parth H. Pathak, Yunze Zeng, Xixi Liran, and Prasant Mohapatra. 2016a. Monitoring vital signs using millimeter wave. In *Proceedings of the 17th ACM International Symposium on Mobile Ad Hoc Networking and Computing (MobiHoc'16)*. ACM, New York, NY, 211–220. DOI: <http://dx.doi.org/10.1145/2942358.2942381>
- Zhicheng Yang, Parth H. Pathak, Yunze Zeng, Xixi Liran, and Prasant Mohapatra. 2016b. Technical Report. Retrieved from <http://spirit.cs.ucdavis.edu/pubs/tr/zhicheng-TOSN-techReport.pdf>.
- Maxim Zhadobov, Nacer Chahat, Ronan Sauleau, Catherine Le Queument, and Yves Le Drean. 2011. Millimeter-wave interactions with the human body: State of knowledge and recent advances. *International Journal of Microwave and Wireless Technologies* 3, 02 (2011), 237–247.
- Xia Zhou, Zengbin Zhang, Yibo Zhu, Yubo Li, Saipriya Kumar, Amin Vahdat, Ben Y. Zhao, and Haitao Zheng. 2012. Mirror mirror on the ceiling: Flexible wireless links for data centers. *ACM SIGCOMM Computer Communication Review* 42, 4 (2012), 443–454.
- Yibo Zhu, Zengbin Zhang, Zhinus Marzi, Chris Nelson, Upamanyu Madhow, Ben Y. Zhao, and Haitao Zheng. 2014. Demystifying 60GHz outdoor picocells. In *Proceedings of the 20th Annual International Conference on Mobile Computing and Networking*. ACM, 5–16.

Received April 2016; revised February 2017; accepted February 2017